NASA/TM—2017-219498

Chemical, Structural, and Microstructural Changes in Metallic and Silicon-Based Coating Materials Exposed to Iodine Vapor

Gustavo C. C. Costa
Vantage Partners, LLC, Brook Park, Ohio

Gabriel F. Benavides and Timothy D. Smith
Glenn Research Center, Cleveland, Ohio

May 2017

NASA STI Program . . . in Profile

Since its founding, NASA has been dedicated to the advancement of aeronautics and space science. The NASA Scientific and Technical Information (STI) Program plays a key part in helping NASA maintain this important role.

The NASA STI Program operates under the auspices of the Agency Chief Information Officer. It collects, organizes, provides for archiving, and disseminates NASA's STI. The NASA STI Program provides access to the NASA Technical Report Server—Registered (NTRS Reg) and NASA Technical Report Server—Public (NTRS) thus providing one of the largest collections of aeronautical and space science STI in the world. Results are published in both non-NASA channels and by NASA in the NASA STI Report Series, which includes the following report types:

- TECHNICAL PUBLICATION. Reports of completed research or a major significant phase of research that present the results of NASA programs and include extensive data or theoretical analysis. Includes compilations of significant scientific and technical data and information deemed to be of continuing reference value. NASA counter-part of peer-reviewed formal professional papers, but has less stringent limitations on manuscript length and extent of graphic presentations.

- TECHNICAL MEMORANDUM. Scientific and technical findings that are preliminary or of specialized interest, e.g., "quick-release" reports, working papers, and bibliographies that contain minimal annotation. Does not contain extensive analysis.

- CONTRACTOR REPORT. Scientific and technical findings by NASA-sponsored contractors and grantees.

- CONFERENCE PUBLICATION. Collected papers from scientific and technical conferences, symposia, seminars, or other meetings sponsored or co-sponsored by NASA.

- SPECIAL PUBLICATION. Scientific, technical, or historical information from NASA programs, projects, and missions, often concerned with subjects having substantial public interest.

- TECHNICAL TRANSLATION. English-language translations of foreign scientific and technical material pertinent to NASA's mission.

For more information about the NASA STI program, see the following:

- Access the NASA STI program home page at http://www.sti.nasa.gov

- E-mail your question to help@sti.nasa.gov

- Fax your question to the NASA STI Information Desk at 757-864-6500

- Telephone the NASA STI Information Desk at 757-864-9658

- Write to:
  NASA STI Program
  Mail Stop 148
  NASA Langley Research Center
  Hampton, VA 23681-2199

NASA/TM—2017-219498

Chemical, Structural, and Microstructural Changes in Metallic and Silicon-Based Coating Materials Exposed to Iodine Vapor

Gustavo C. C. Costa
Vantage Partners, LLC, Brook Park, Ohio

Gabriel F. Benavides and Timothy D. Smith
Glenn Research Center, Cleveland, Ohio

National Aeronautics and
Space Administration

Glenn Research Center
Cleveland, Ohio 44135

May 2017

Acknowledgments

The following work was conducted under the Advanced In-Space Propulsion (AISP) project with support from NASA's Game Changing Development Program within the Space Technology Mission Directorate (STMD). We would like to thank Dr. R. Rogers (NASA Glenn) for assistance with the X-ray diffraction measurements. We would also like to thank the Silcotek Corporation for providing Silcolloy® and Dursan® coating of provided material test coupons for our evaluation.

This report contains preliminary findings, subject to revision as analysis proceeds.

Level of Review: This material has been technically reviewed by technical management.

Available from

NASA STI Program
Mail Stop 148
NASA Langley Research Center
Hampton, VA 23681-2199

National Technical Information Service
5285 Port Royal Road
Springfield, VA 22161
703-605-6000

This report is available in electronic form at http://www.sti.nasa.gov/ and http://ntrs.nasa.gov/

Contents

Chemical, Structural, and Microstructural Changes in Metallic and Silicon-Based Coating Materials Exposed to Iodine Vapor

Gustavo C. C. Costa
Vantage Partners, LLC
Brook Park, Ohio 44142

Gabriel F. Benavides and Timothy D. Smith
National Aeronautics and Space Administration
Glenn Research Center
Cleveland, Ohio 44135

Summary

The chemical, structural, and microstructural behavior of steels (304, 316, and A36), titanium-aluminum alloy (Ti-Al or Al-Ti (6Al-4V)), aluminum-magnesium alloy (Al-Mg (Al-6061)), and coatings (Silcolloy® and Dursan® (SilcoTek Corporation)) were probed after exposure to iodine laminar flow. Exposures were carried out in a custom-built Iodine Vapor RIG (IVR) at 300 °C to an iodine laminar vapor flow of 1 $mg \cdot min^{-1}$, carried by 145 $mL \cdot min^{-1}$ argon gas, for 5, 15, and 30 days. Samples were characterized before and after the experiment by gravimetric analysis, X-ray diffraction (XRD) and cross section electron microscopy analysis coupled with energy dispersive X-ray spectroscopy (EDS). All steels exposed for 30 days formed scales consisting mainly of metal (Cr, Fe, and Ni) oxides showing different chemistry, microstructure, and crystalline phases. Elemental iodine was only detected by EDS analysis in the scales of stainless steels 304 and 316. After 30 days, the Ti-Al exhibited no detectable scale, suggesting only a very thin film was formed. A scale consisting mainly of aluminum, iodine, and oxygen formed on the Al-Mg sample exposed for 30 days. Some pockets rich in magnesium, iodine, and oxygen also formed in this Al-Mg alloy. Stainless steel 316, low carbon steel A36, and Ti-Al alloy coated with Silcolloy® and stainless steel 304 coated with Dursan® that were exposed for 30 days exhibited no oxidation. Stainless steel 304 coated with Silcolloy® exposed for 30 days did not exhibit corrosion although the sample gained weight and the coating exhibited expansion. The weight gain per area performance of the materials exposed in iodine lamina flow containing oxygen at impurity level for 10, 15, and 30 days are reported from the lowest to the highest weight gain per area as follows: Steels: < 316 < 304 < A36; Ti-Al-Mg-based alloys: Al-Mg < Ti-Al: Considering the experimental uncertainties, no weight change was observed for stainless steel 316, low carbon steel A36, and Ti-Al alloy coated with Silcolloy® and stainless steel 304 coated with Dursan®. The corrosion of the alloys is catalyzed by iodine in the presence of oxygen as impurity.

Introduction

NASA Glenn Research Center is currently performing development of iodine Hall Effect Thruster (HET) propulsion technology under two programs. The Iodine Satellite (iSat) project is funded through NASA's Small Spacecraft Technology Program (SSTP), and a 600-W iodine HET is being developed under the Advanced In-Space Propulsion (AISP) project funded through NASA's Game Changing Development Program within the Space Technology Mission Directorate (STMD) (Ref. 1). Both projects employ vaporized iodine as the propellant. NASA Glenn has demonstrated that Hall thrusters operating on iodine propellant perform at the same thrust and efficiency compared to operation of state-of-the-art xenon propellant (Ref. 1). This is remarkable because iodine has many storage benefits when compared with xenon (Refs. 2 and 3). First, iodine stores at 3 times the density of xenon. A greater storage density allows for greater propellant mass carried on volume limited spacecraft, which results in a greater propulsive capability. Second, iodine stores at less than 15 psia, as opposed to 2500 psi for xenon.

Low-pressure storage simplifies tankage design, permits use of conformal tank geometries to optimize spacecraft volume utilization, and reduces launch safety concerns. Lastly, iodine is much more abundant and as a result far less costly to acquire than xenon propellant. These are key factors that make iodine an important alternative propellant to xenon for low-cost, volume-constrained missions under consideration. However, some engineering challenges must first be addressed.

Foremost amongst these challenges is addressing material compatibility (Ref. 1) of the propulsion system, the spacecraft, and test facilities. Little is known regarding iodine reactivity with the wide range of spacecraft materials in a vacuum environment. Without such understanding, acceptance of iodine as a viable alternative to xenon is not possible, regardless of its demonstrated performance benefits. Furthermore, the interaction between iodine and a wide diversity of materials is of interest in nuclear materials science. Iodine is regarded as one of the most hazardous fission products from a fuel nuclear reactor and experimental data on the interaction between iodine and alloys (e.g., stainless steel 304) can be used to predict the iodine interaction with the containment in a case of nuclear accident.

The goal of this work is to begin studying the chemistry, structure, and microstructural and kinetics properties of materials and coatings exposed to iodine in a relevant environment to spacecraft technology development. For the study described in this report, five common spacecraft and test facility metals (stainless steels 304 and 316, low carbon steel A36, and alloys 6Al-4V and AL-6061), and two coatings (Silcolloy® and Dursan® (SilcoTek Corporation)) were selected. The two coatings are amorphous hydrogen-passivated, silicon- and carboxysilane-based coatings. The results of this work are pertinent to vacuum facilities (~10^{-6} torr) and some regions of space (low Earth orbit) since these environments contain molecular or atomic oxygen at very low levels. We also use FactSage and associated databases (Refs. 4 and 5) as a thermochemistry computational tool to calculate the main compounds formed at their thermodynamic equilibrium with iodine vapor and/or low levels of oxygen.

Experimental

Materials

The materials used in this work are divided into two groups: Group I—Metallic materials consisting of 304 and 316 stainless steels, A36 low carbon steel, Al-6061 aluminum alloy, and 6Al-4V TiAl alloy. Steels and aluminum sheets were purchased at McMaster-CARR® and TiAl alloy at RTI International Metals, Inc. The metallic sheets were cut in 0.5- by 0.5-in. square shapes with 0.075-in. orifices (Figure 1). Group II—Coatings consisting of Silcolloy® (silicon-based coating material and oxidation resistant up to 1000 °C) and Dursan® (silicon-based coating material functionalized with oxygen and carbon and corrosion and abrasion resistant up to 450 °C). Both coatings were applied on the samples by SilcoTek. The coating Silcolloy® was applied on the steels 304, 316, and A36 and on TiAl alloy. Dursan® coating was also applied on stainless steel 304.

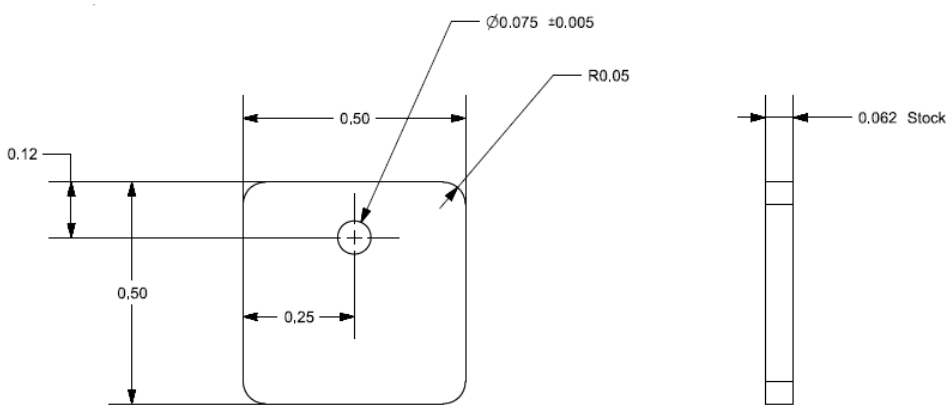

Figure 1.—Sample coupon dimensions.

All samples were cleaned with a detergent solution, rinsed with deionized water, and ultrasonicated in acetone and ethanol prior to the experiments. Samples were weighed on an analytical balance (Sartorius model 1712 MP8) (±0.0003) before and after the exposure to the iodine vapor laminar flow.

Exposure Procedure in Iodine Vapor Laminar Flow

Triplicate samples of each material were placed on a sample holder illustrated in Figure 2. The sample holder consisted of a semicircular alumina tube with gold wires suspended perpendicular on the tube. Samples were directly suspended from the gold rod using alumina spacers to separate them. This sample holder was placed inside of the quartz tube of the tubular furnace. The furnace was sealed and flushed with argon at 145 mL·min^{-1} while the temperature was raised to 300 °C and kept for about 1 h before the iodine/argon laminar flow (Figure 3). The experiment started when an empty Erlenmeyer flask sitting on a hot plate at ~50 °C was replaced by another Erlenmeyer flask containing solid iodine. The Erlenmeyer flask containing iodine was replaced by an empty one to stop the iodine flow at the end of the experiment. Each batch of triplicate coupon samples were exposed to an iodine laminar vapor flow of 1 mg·min^{-1}, carried by 145 mL·min^{-1} argon gas, for 5, 15, and 30 days.

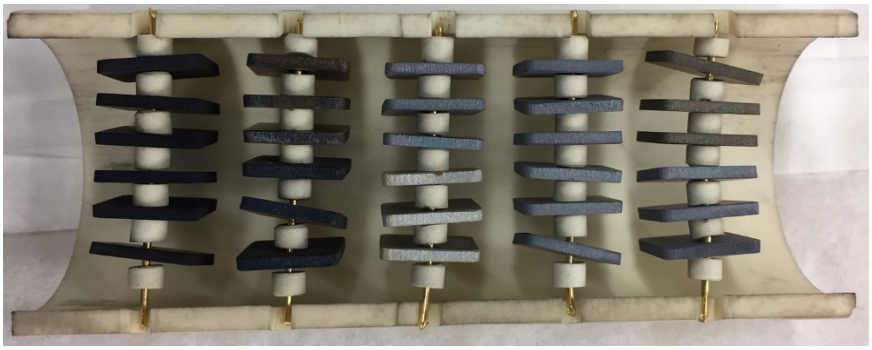

Figure 2.—Alumina sample holder with coupon samples perpendicular suspended with gold wires. Samples were separated by alumina spacers.

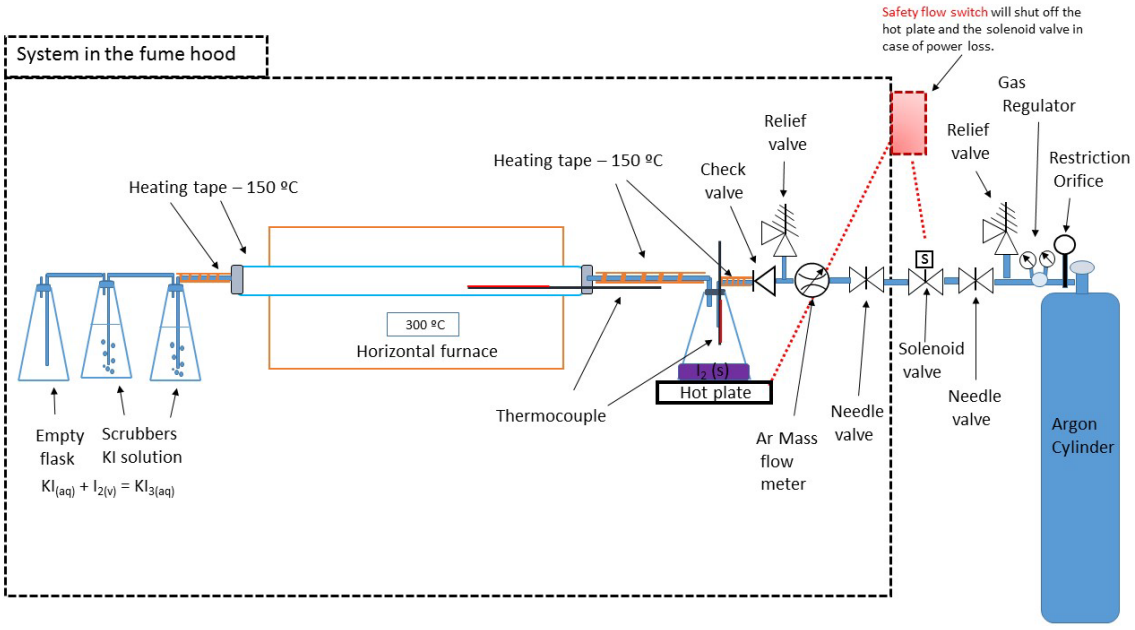

Figure 3.—Iodine Vapor RIG system—Argon carrier gas flows at 145 mL·min^{-1} through Erlenmeyer flask containing solid/vapor iodine heated at ~50 °C. Iodine vapor is carried by argon through heated stainless steel lines kept at ~150 °C and quartz tube inserted in tubular furnace heated at 300 °C. Iodine vapor retained as potassium triiodide in 0.1 mol·L^{-1} potassium iodide solution.

Sample Characterization

After exposure the samples were analyzed by X-ray diffraction (XRD) on a Panalytical Empyrean diffractometer (PANanalytical B.V.) and by Field Emission Scanning Electron Microscope (FE–SEM) Hitachi S4700–II (Hitachi High Technologies) equipped with energy dispersive X-ray spectroscopy (EDS) (EDAX, Inc.), a secondary electron detector (SED), and a backscatter electron detector (BSE). For FE–SEM analysis, samples were mounted in a PolyFast® resin, polished using a nonaqueous solution. A Focused Ion Beam Scanning Electron Microscope (FIB–SEM) equipped with GEMINI electron beam column (Carl Zeiss AG) was also used to characterize some of the coated samples. The coupon samples were weighed before and after exposure to iodine and then normalized to the unit area by dividing the weight change by the total area of a particular sample. This analysis is used to determine weight gain or loss per area of the samples due to reactions occurring between the iodine vapor and the solid phase. The assessment of the results of the gravimetric analysis of the triplicate samples can be used to determine the potential material candidates for use in an iodine atmospheric condition.

Results

Gravimetric Analysis and Kinetics of Reaction

A weight gain per area was observed for the steel samples exposed to iodine laminar flow (Figure 4). This weight gain is usually related to scale or oxide growth. Stainless steel 316 exhibited the lowest weight gain per area followed by stainless steel 304 and carbon steel A36 when individual data points are compared. The weight per area of carbon steel A36 increased 0.7 ± 0.1 mg cm^{-2} from 5 to 15 days and decreased 0.7 ± 0.1 mg cm^{-2} from 15 to 30 days. From 5 to 30 days, the weight gain per area of stainless steels 304 and 316 slightly increased by 0.2 ± 0.1 mg cm^{-2} and 0.3 ± 0.1 mg cm^{-2}, respectively. Additional data points are required to calculate the weight gain rate of the steel samples.

Figure 5 shows the weight loss per area of Al-6061 aluminum alloy and 6Al-4V TiAl alloy samples. A slight decrease of 0.5 ± 0.1 mg cm^{-2} in the weight of the TiAl sample is observed from 5 to 15 days. At the same exposure lengths, the AlMg alloy sample had a much more pronounced weight loss of 2.0 ± 0.1 mg cm^{-2}. The weight loss (11.6 ± 0.1 mg cm^{-2} – TiAl and 8.4 ± 0.1 mg cm^{-2} – AlMg) for these samples are much steeper from 15 to 30 days.

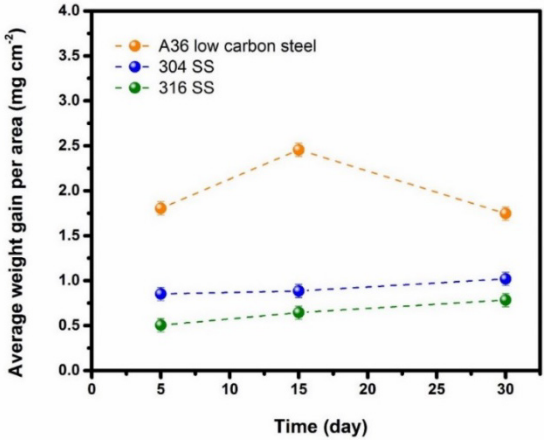

Figure 4.—Weight change per area vs. time for steels exposed to iodine laminar flow at 300 °C. Dash line is added to act as guide to eyes.

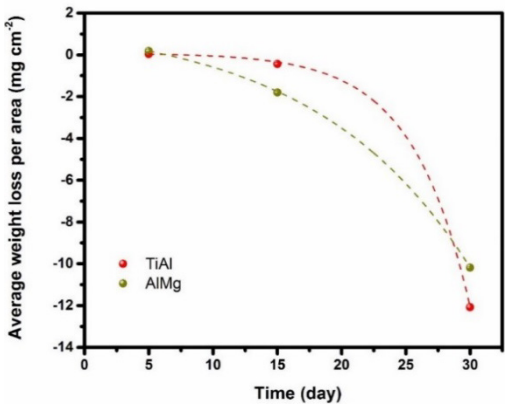

Figure 5.—Weight change per area vs. time for alloys 6Al-4V (TiAl) and Al-6061 (aluminum containing ~1 wt% Mg) exposed to iodine laminar flow at 300 °C. Dash line is added to act as guide to eyes.

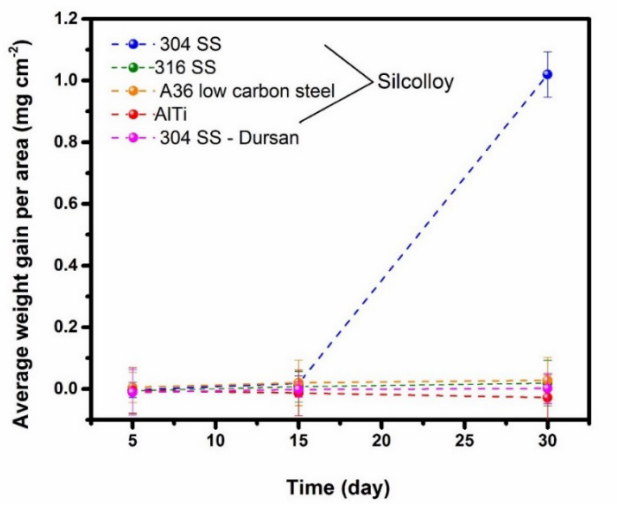

Figure 6.—Weight change per area vs. time for alloys coated with Silcolloy® and Dursan® silicon-based coatings exposed to iodine laminar flow at 300 °C. Dash line is added to act as guide to eyes.

Allowing for experimental error, no weight change was observed for the samples stainless steel 316, carbon steel A36, and AlTi coated with Silcolloy® and for the stainless steel 304 sample coated with Dursan® exposed to the iodine laminar flow (Figure 6). Only the stainless steel 304 sample coated with Silcolloy® exhibited a weight gain of 1.02 ± 0.07 mg cm^{-2}.

Cross Section Microstructural, Structural, and Surface Characterization Alloys

Cross-sectional analysis using scanning electron microscopy (SEM) coupled with energy-dispersive X-ray spectroscopy (EDS) was used to probe possible microstructural (e.g., oxide/iodate layer(s) if present) and elemental changes in the materials exposed to the iodine vapor laminar flow. The SEM–EDS analysis results presented in this work are for samples exposed in an iodine vapor laminar flow for 30 days. The EDS results for this work are semiquantitative and in some cases carbon was detected in all samples due to adsorption of residual carbon dioxide present in the SEM chamber even at low vacuum.

The cross-sectional SEM and BSE images of the as-received (reference) and exposed stainless steel 304 coupon samples are shown in Figure 7 and Figure 8, respectively. Figure 8 shows a scale exhibiting dark and bright areas formed on the stainless steel 304 sample exposed to iodine for 30 days. This scale is 6.8 ± 0.4 μm thick and it is well bonded to the sample.

The results of the EDS elemental analysis performed on the reference and exposed stainless steel 304 samples are presented in Figure 9 and Table 1. Spot EDS elemental analysis performed on the scale detected high contents of iron (66 wt%) and oxygen (30.2 wt%) and low contents of chromium (2.3 wt%) and nickel (1.9 wt%) in the bright area. Alternatively, high contents of iron (29 wt%), chromium (36 wt%), and oxygen (30.4 wt%), and low contents of nickel (4.6 wt%) were detected by EDS in the dark area. Beside high contents of iron (44 wt%), chromium (17.5 wt%) and oxygen (28.6 wt%), minor amounts of iodine (1.7 wt%), and molybdenum (1.3 wt%) were also detected in bright layer at the alloy-oxide interface. The elemental compositions of the bulk of the reference and the exposed samples are the same within the experimental uncertainties.

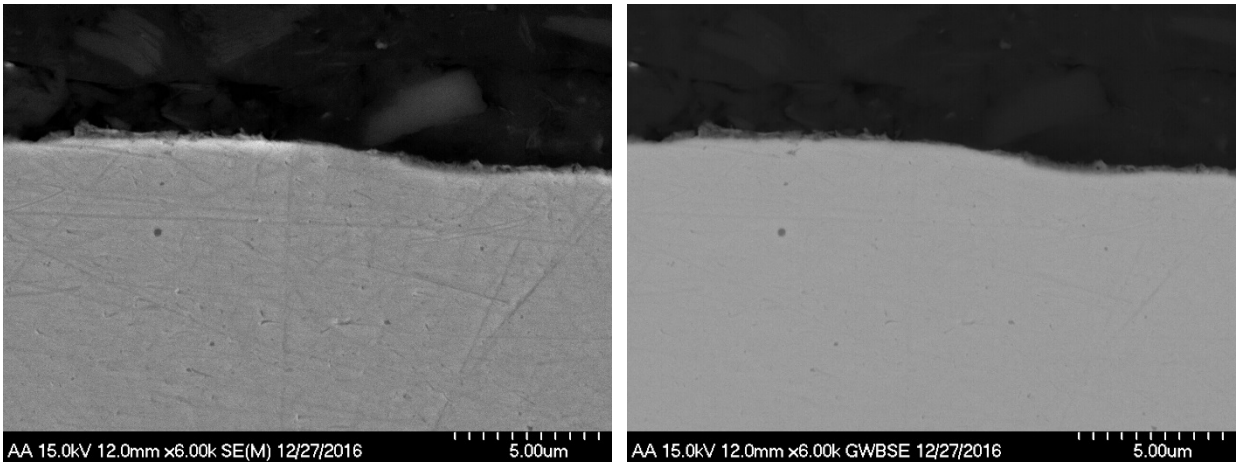

(a) (b)

Figure 7.—Cross-sectional reference stainless steel 304 coupon sample. (a) SEM. (b) BSE.

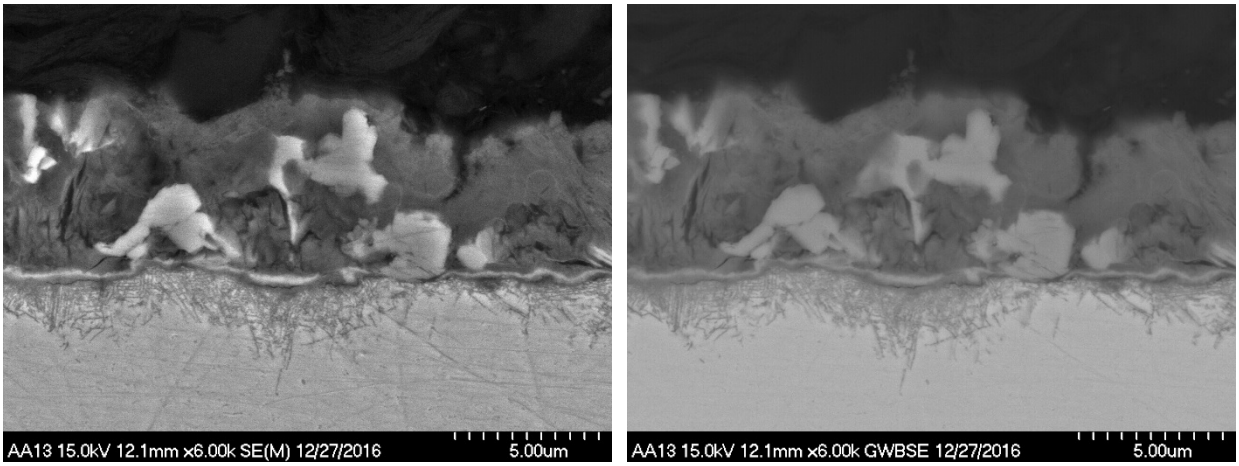

(a) (b)

Figure 8.—Cross-sectional stainless steel 304 coupon sample that was exposed to iodine laminar vapor flow for 30 days. (a) SEM. (b) BSE.

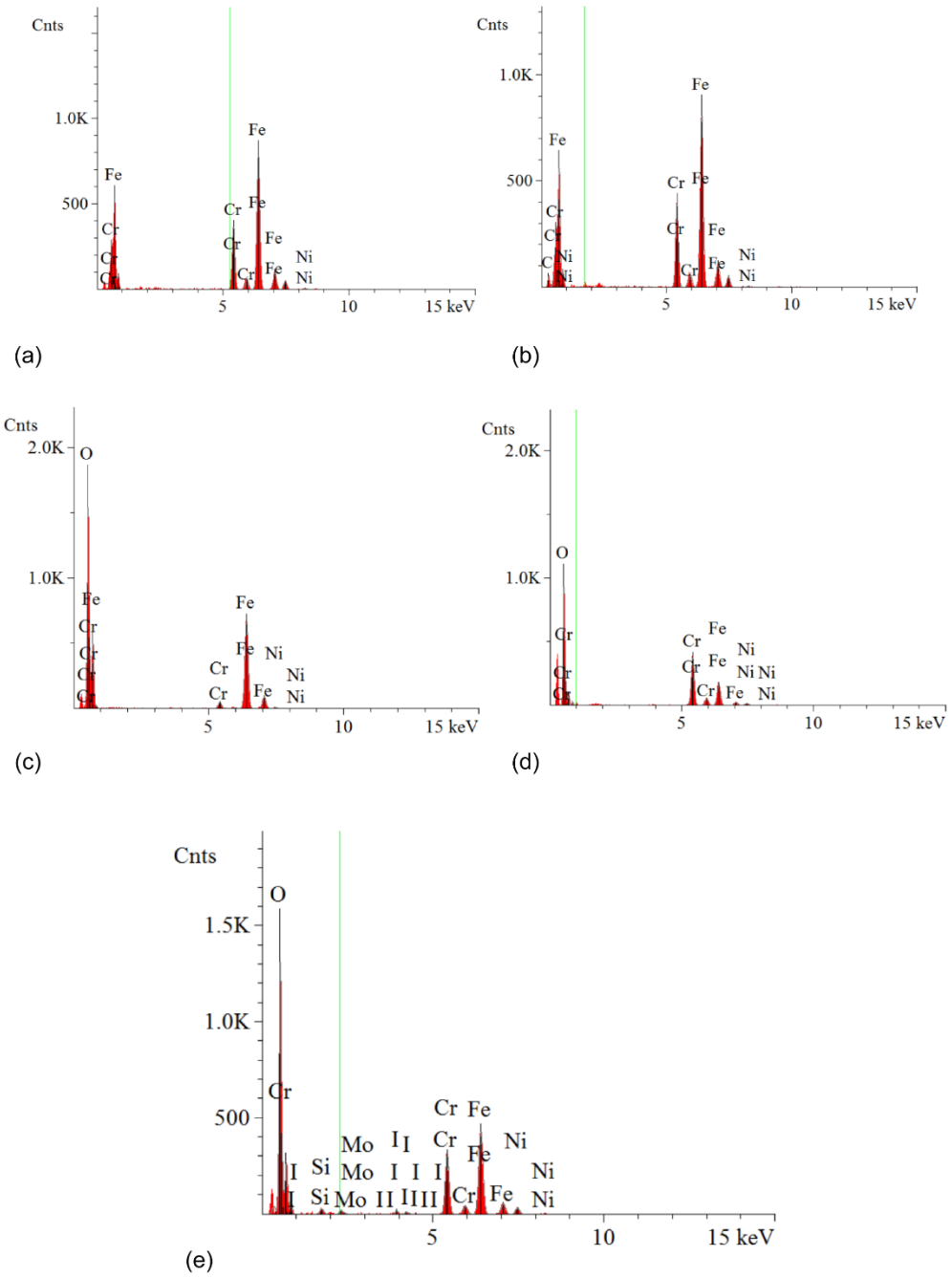

Figure 9.—EDS analysis of stainless steel 304 samples. (a) Bulk of reference. (b) Bulk of exposed sample for 30 days. (c) Bright. (d) Dark areas. (e) Interface of scale on exposed sample.

TABLE 1.—CHEMICAL COMPOSITION OBTAINED FROM EDS ANALYSIS OF BULK OF REFERENCE STAINLESS STEEL SAMPLE AND OF BULK AND SCALE OF SS304 COUPON SAMPLE EXPOSED TO IODINE LAMINAR VAPOR FLOW FOR 30 DAYS

Element	Weight (%)				
	Reference bulk	Exposed bulk	Interface (oxide/bulk)	Scale (bright area)	Scale (dark area)
Fe	74(1)	74(1)	44(1)	66(1)	29(1)
Cr	17.9(5)	18.2(5)	17.5(5)	2.3(2)	36(1)
Ni	8.3(7)	8.0(7)	6.0(5)	1.9(5)	4.6(8)
Mo	--------	--------	1.3(4)	--------	--------
I	--------	--------	1.7(4)	--------	--------
O	--------	--------	28.6(6)	30.2(5)	30.4(7)

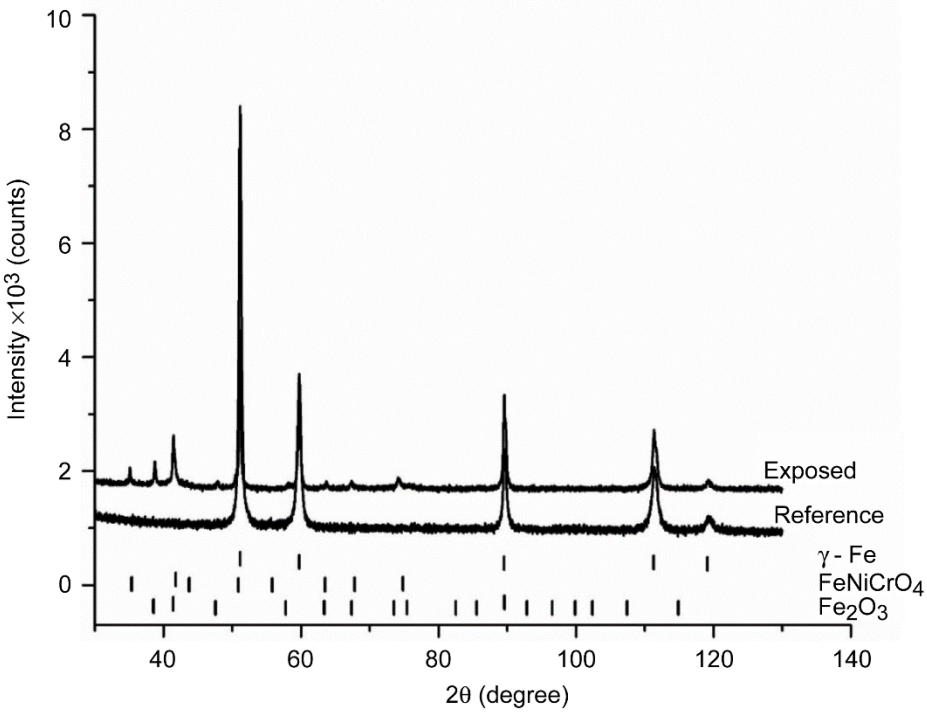

Figure 10.—X-ray diffraction patterns of stainless steel 304 samples unexposed and exposed to iodine vapor laminar flow for 30 days.

The XRD patterns of the stainless steel 304 samples both unexposed and exposed to iodine for 30 days are presented in Figure 10. Only γ austenite (PDF card # 04-002-3692) phase was detected by XRD analysis in the as-received sample. Hematite (Fe_2O_3, PDF card # 00-001-1053) and nickel chromium iron oxide ($NiCrFeO_4$, PDF card # 00-052-0068) phases were detected on the sample exposed in iodine vapor laminar flow beyond the γ phase.

Figure 11 and Figure 12 show the cross-sectional SEM and BSE images of the as-received (reference) and exposed stainless steel 316 coupon samples, respectively. A 3.8 ± 0.3-μm-thick scale formed on the alloy (Figure 12). This scale is detached and not well bonded to the base of the sample, which is detrimental for corrosion resistance of the alloy.

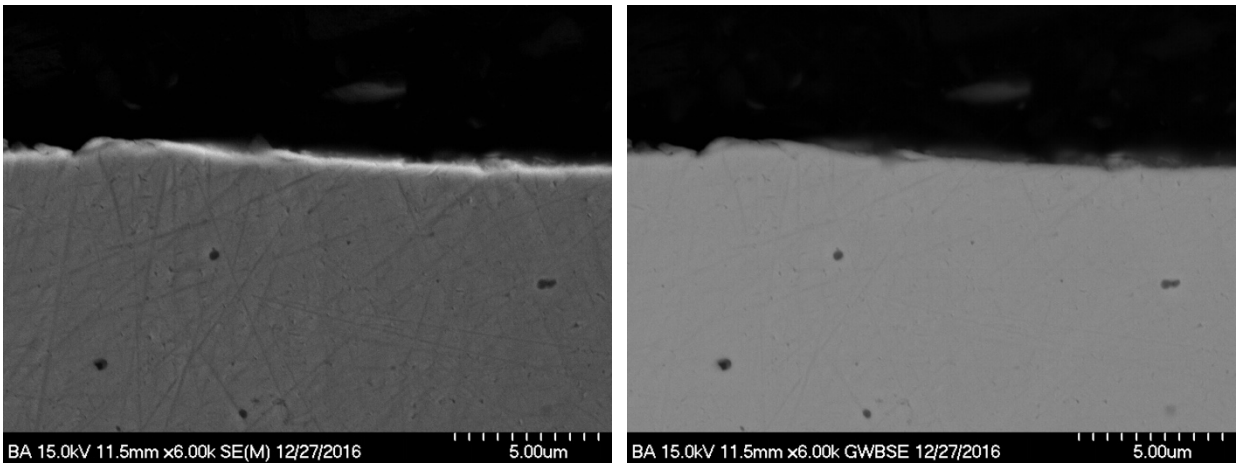

(a) (b)

Figure 11.—Cross-sectional of reference stainless steel 316 coupon sample. (a) SEM. (b) BSE.

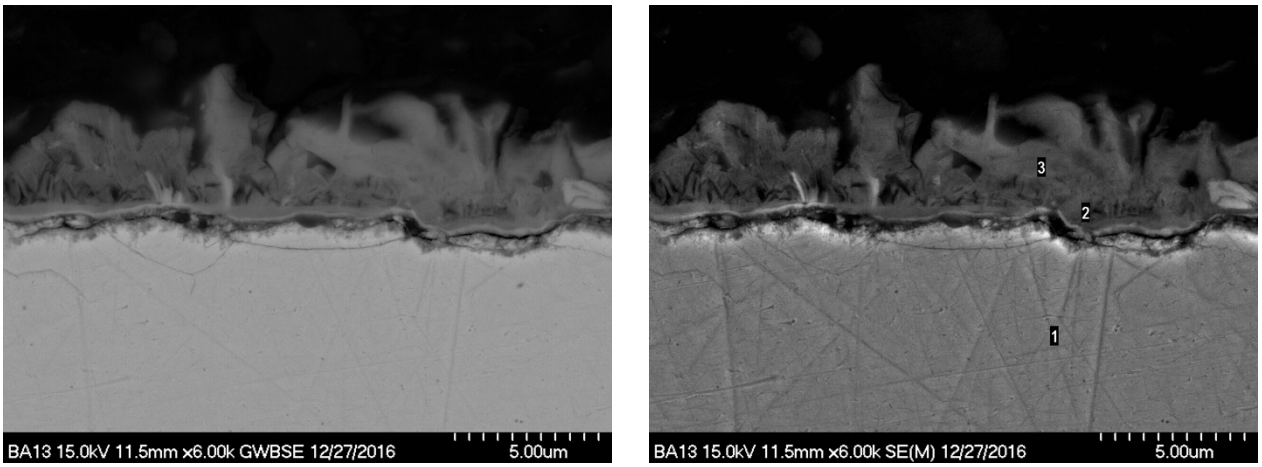

(a) (b)

Figure 12.—Cross-sectional stainless steel 316 coupon sample exposed to iodine laminar vapor flow for 30 days. (a) SEM. (b) BSE.

The EDS elemental analyses are shown in Figure 13, and the weight percentage of the elements are presented in Table 2. High contents of iron (38 wt%), chromium (15 wt%), nickel (13 wt%), and oxygen (30.4 wt%), and low contents of iodine (3.6 wt%), molybdenum (2.0 wt%), and silicon (0.4 wt%) were detected by EDS in the scale. The elemental compositions of the bulk of the reference and exposed samples are the same within the experimental uncertainties.

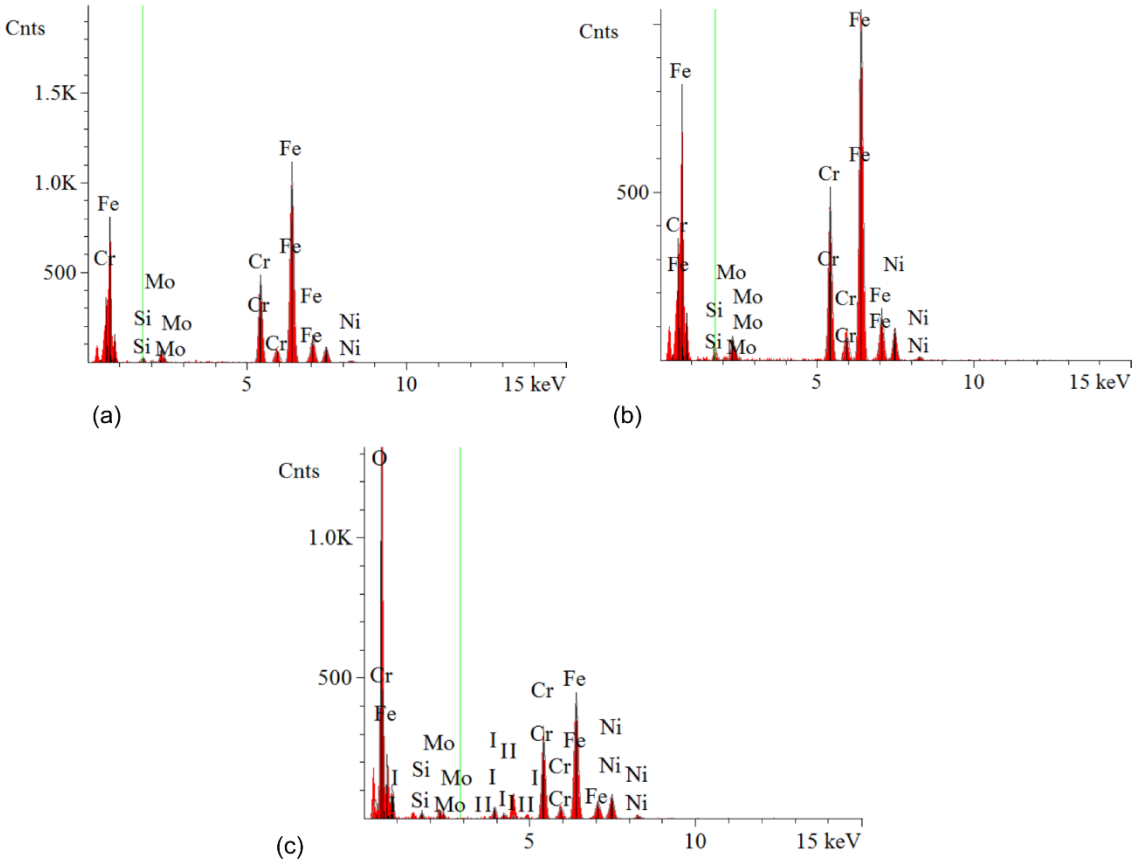

Figure 13.—EDS analysis of stainless steel 316 samples. (a) Bulk of reference. (b) Bulk of exposed sample for 30 days. (c) Scale on exposed sample.

TABLE 2.—CHEMICAL COMPOSITION OBTAINED FROM EDS ANALYSIS OF THE BULK OF THE REFERENCE SS316 SAMPLE AND OF BULK AND SCALE OF SS316 COUPON SAMPLE EXPOSED TO IODINE LAMINAR VAPOR FLOW FOR 30 DAYS

Element	Weight (%)		
	Reference bulk	Exposed bulk	Scale
Fe	70(1)	69(1)	38(1)
Cr	16.3(4)	16.6(4)	14.5(5)
Ni	10.5(7)	10.6(7)	12.8(1)
Mo	2.8(4)	3.0(4)	2.0(4)
Si	0.4(1)	0.6(1)	0.4(1)
O	--------	--------	29.0(5)
I	--------	--------	3.6(5)

The XRD patterns of the stainless steel 316 samples both unexposed and exposed to iodine for 30 days are presented in Figure 14. The stainless steel 316 sample exposed to iodine vapor exhibited the same evolution of phases to that in the stainless steel 304 sample. XRD analysis detected only γ austenite (PDF card # 04-002-3692) phase in the as-received sample. Hematite (Fe_2O_3, PDF card # 00-001-1053) and nickel chromium iron oxide ($NiCrFeO_4$, PDF card # 00-052-0068) phases were also detected by XRD on the sample exposed in iodine vapor beyond the γ phase.

Figure 15 and Figure 16 show the cross-sectional SEM and BSE images of the as-received (reference) and exposed A36 low carbon steel coupon samples, respectively. The scale formed on the alloy (Figure 16) consists of three layers and is 42 ± 5 μm thick. The scale is detached from the base of the alloy and its first layer is slightly porous.

The EDS elemental analyses are shown in Figure 17 and the weight percentage of the elements are presented in Table 3. The lower and upper layer are rich in iron (65 wt% and 71 wt%) and oxygen (32.1 wt% and 29.9 wt%). The intermediate is also rich in carbon (14.7 wt%) besides iron (61 wt%) and oxygen (24.2 wt%). The elemental compositions of the bulk of the reference and exposed samples are the same within the experimental uncertainties.

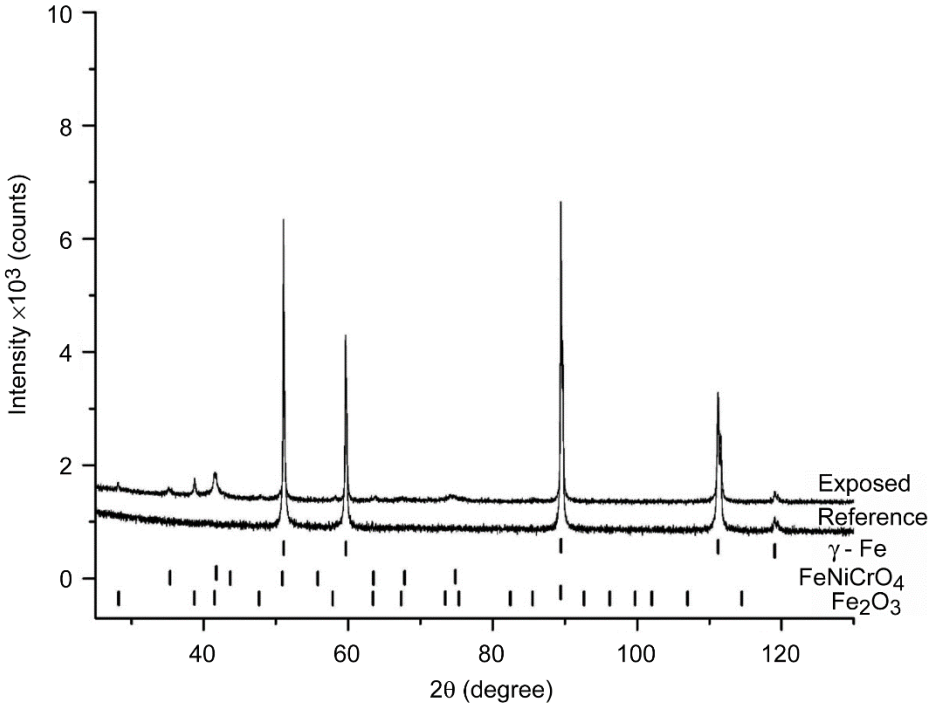

Figure 14.—X-ray diffraction patterns of stainless steel 316 samples unexposed and exposed to iodine vapor laminar flow for 30 days.

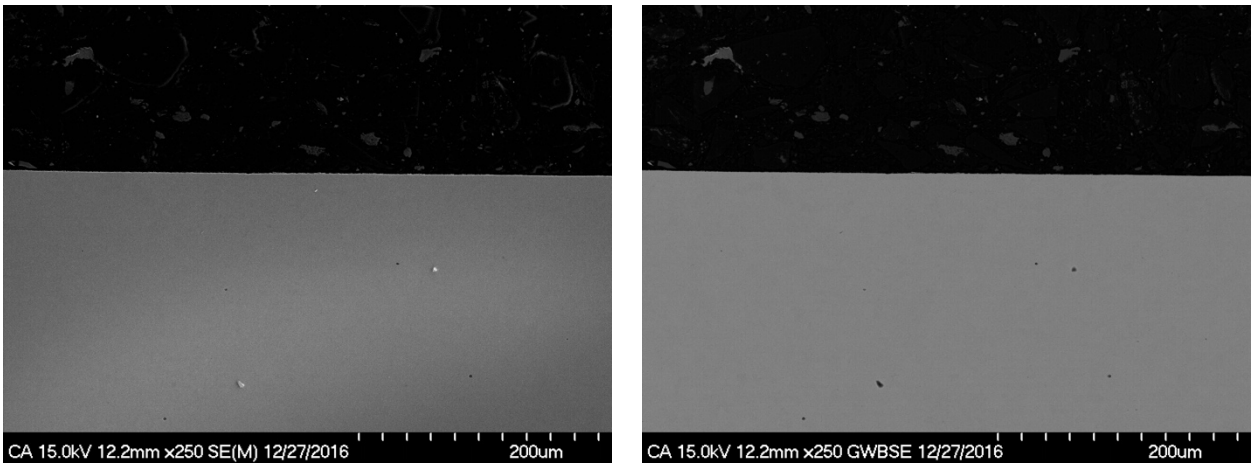

(a) (b)

Figure 15.—Cross-sectional reference A36 low carbon steel coupon sample. (a) SEM. (b) BSE.

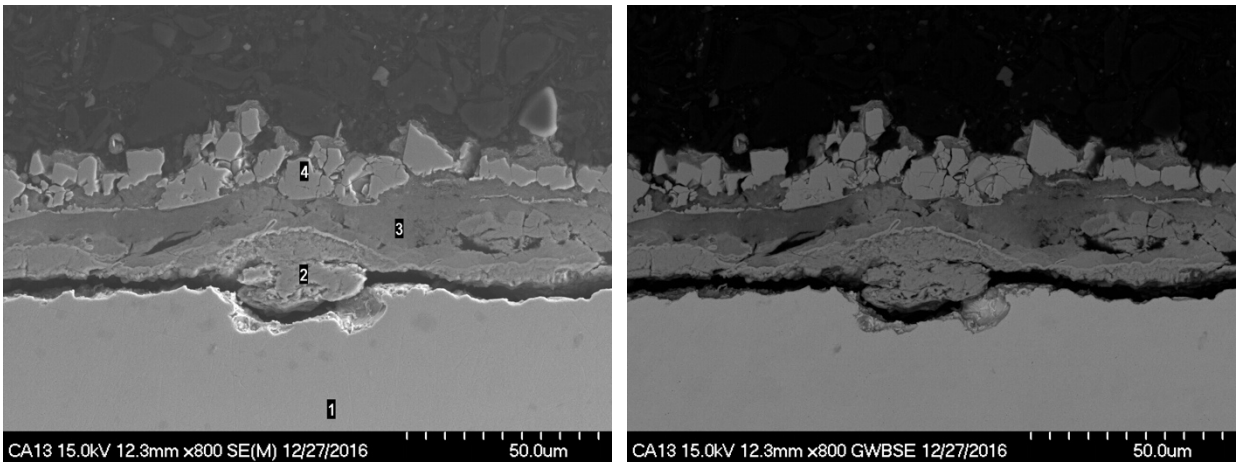

(a) (b)

Figure 16.—Cross-sectional A36 low carbon steel coupon sample exposed to iodine laminar vapor flow for 30 days. (a) SEM. (b) BSE.

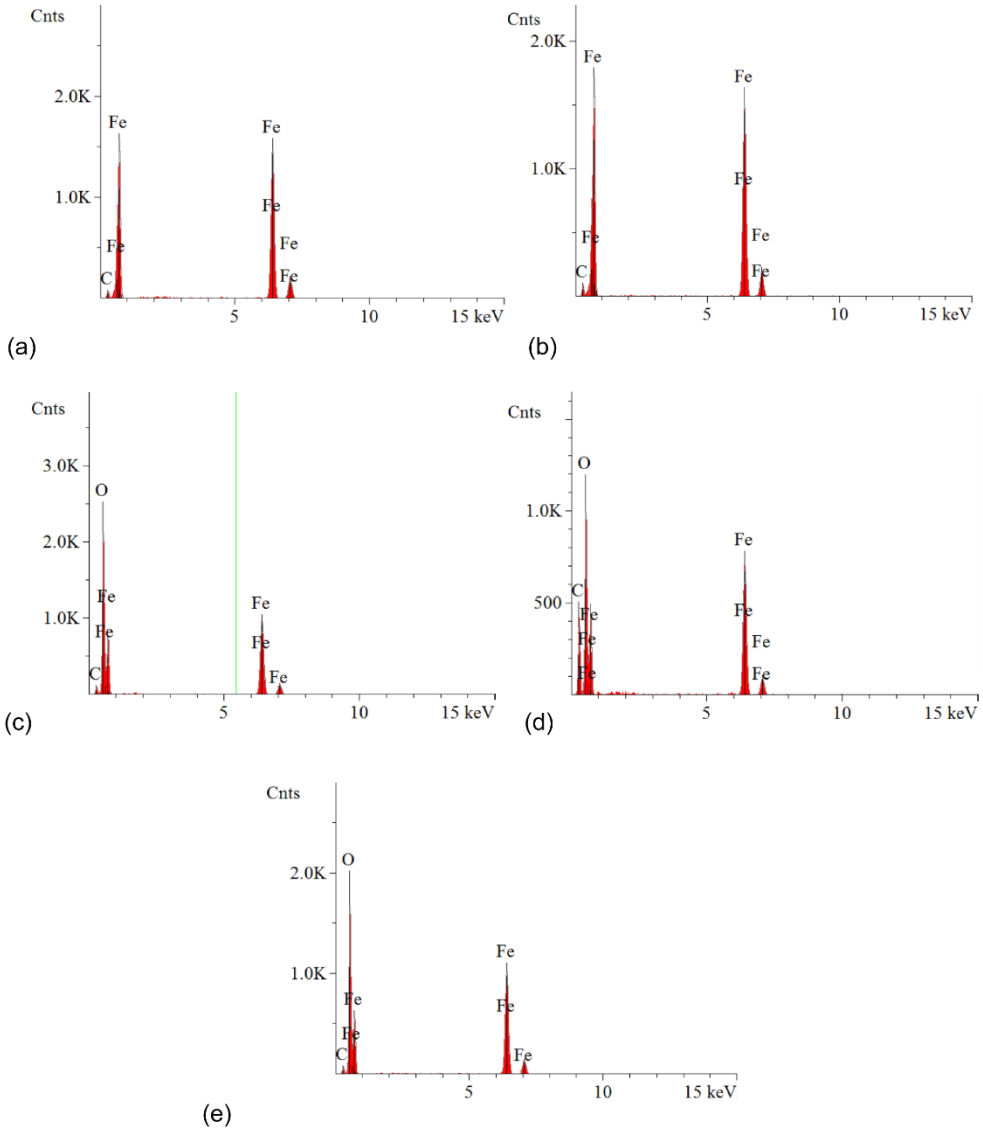

Figure 17.—EDS analysis of A36 low carbon steel samples. (a) Bulk of reference. (b) Bulk of exposed sample for 30 days. (c) Lower layer (Figure 16a-2). (d) Intermediate layer (Figure 16a-3). (e) Upper layer of scale (Figure 16a-4).

TABLE 3.—CHEMICAL COMPOSITION OBTAINED FROM EDS ANALYSIS OF BULK OF REFERENCE A36 LOW CARBON STEEL COUPON SAMPLE AND OF BULK AND SCALE OF A36 LOW CARBON STEEL COUPON SAMPLE EXPOSED TO IODINE LAMINAR VAPOR FLOW FOR 30 DAYS

Element	Weight (%)				
	Reference bulk	Exposed bulk	Inner layer	Middle layer	Outer layer
Fe	97(1)	97(1)	65(1)	61(1)	71(1)
C	2.9(4)	3.3(3)	3.1(3)	14.7(5)	2.4(3)
O	-------	-------	32.1(5)	24.2(5)	29.9(4)

The XRD patterns of the A36 low carbon steel samples both unexposed and exposed to iodine vapor for 30 days are presented in Figure 18. XRD analysis detected only α ferrite (PDF card # 98-000-1720) phase in the as-received sample. Magnetite (Fe_3O_4, PDF card # 04-012-7038) and maghemite ($Fe_{2.66}O_4$, PDF card # 98-001-6961) phases were detected by XRD on the sample exposed in iodine vapor beyond the α phase.

Figure 19 and Figure 20 show the cross-sectional SEM and BSE images of the as-received (reference) and exposed TiAl alloy coupon samples, respectively. Microstructural changes such as formation of scales/secondary phases, microcracks, flaking, etc., were not observed for the TiAl alloy sample exposed in iodine vapor laminar flow for 30 days.

The EDS elemental analyses are shown in Figure 21, and the weight percentage of the elements are presented in Table 4. EDS elemental analysis of the TiAl alloys detected solely their constituent elements. The elemental compositions of the reference and exposed samples are the same within the experimental uncertainties.

The XRD patterns of the TiAl alloy samples both unexposed and exposed to iodine vapor for 30 days are presented in Figure 22. XRD analysis detected the α phase (PDF card # 04-004-9156) and titanium suboxide phase ($TiO_{0.45}$, PDF card # 01-089-3074) in the as-received sample. Anatase (TiO_2, PDF card # 98-000-0081) phases was detected by XRD on the sample exposed in iodine vapor beyond the α and suboxide phases.

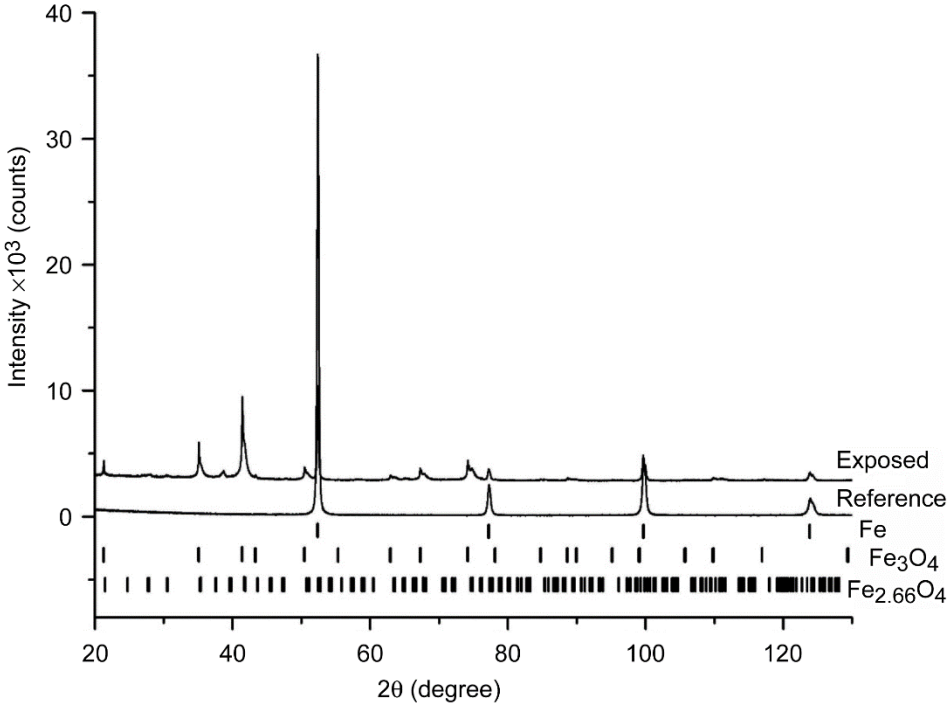

Figure 18.—X-ray diffraction patterns of A36 low carbon steel samples unexposed and exposed to iodine vapor laminar flow for 30 days.

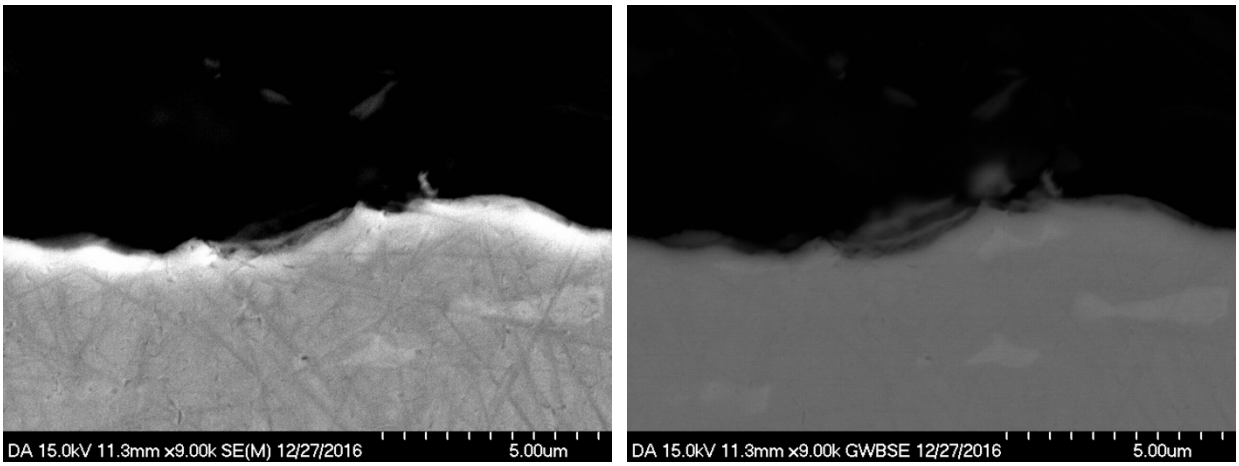

(a) (b)

Figure 19.—Cross-sectional reference TiAl alloy coupon sample. (a) SEM. (b) BSE.

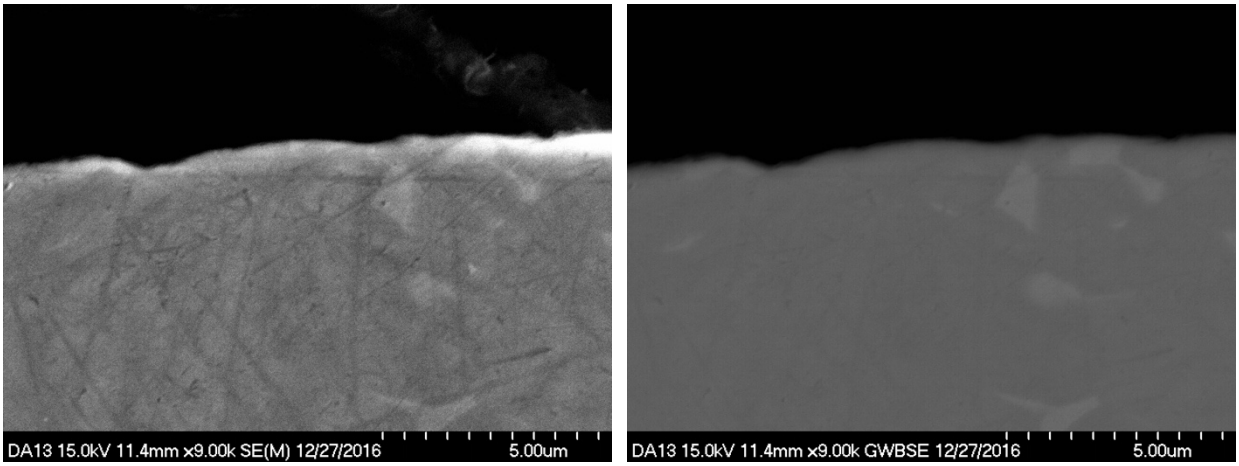

(a) (b)

Figure 20.—Cross-sectional TiAl alloy coupon sample exposed to the iodine laminar vapor flow for 30 days. (a) SEM. (b) BSE.

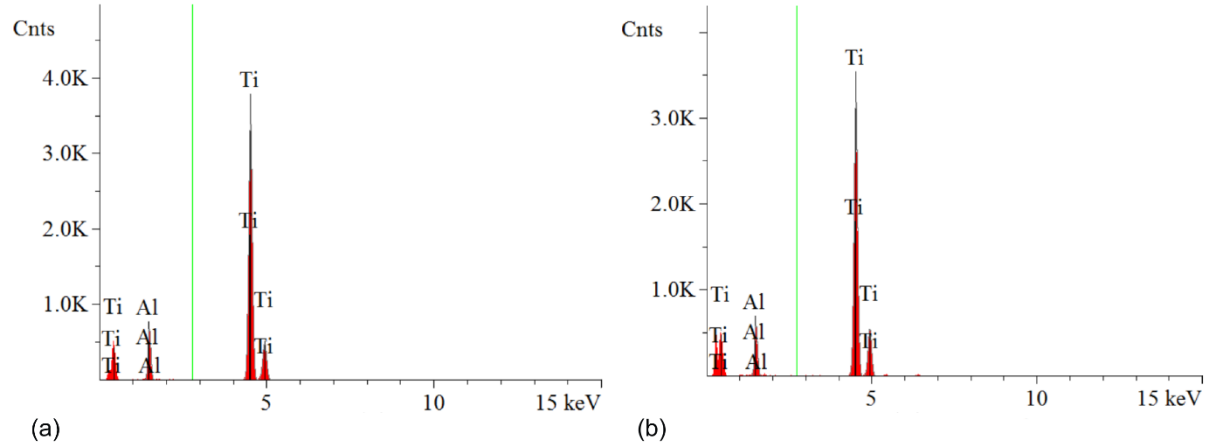

(a) (b)

Figure 21.—EDS analysis of TiAl alloy samples. (a) Reference. (b) Exposed for 30 days.

TABLE 4.—CHEMICAL COMPOSITION OBTAINED FROM EDS ANALYSIS OF BULK OF REFERENCE AND EXPOSED TiAl ALLOY SAMPLES

Element	Weight (%)	
	Reference bulk	Exposed bulk
Ti	92.4(9)	92.7(9)
Al	7.2(6)	7.3(2)

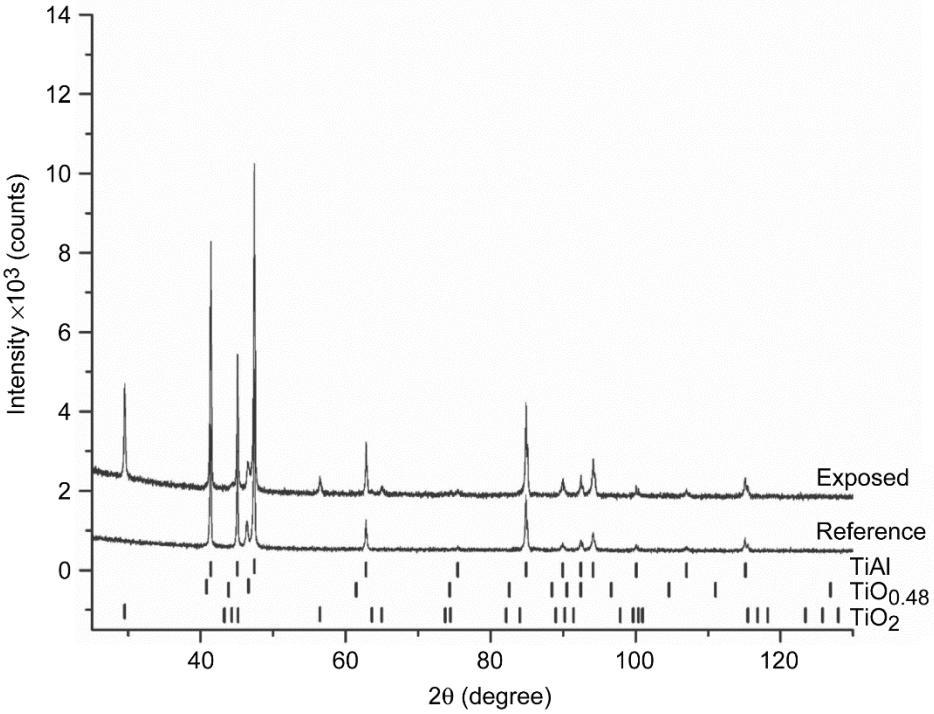

Figure 22.—X-ray diffraction patterns of TiAl alloy samples unexposed and exposed to iodine vapor laminar flow for 30 days.

Figure 23 and Figure 24 show the cross-sectional SEM and BSE images of the as-received (reference) and exposed 6061 aluminum alloy coupon samples, respectively. A 4.1 ± 5-μm-thick scale formed on the alloy (Figure 24). There are also areas of "pockets" of oxidation in the bulk of the alloy and small dark areas or spots in the bulk of the sample. The small dots are an indication of preferential chemical affinity of magnesium of the alloy to the residual oxygen in the iodine vapor phase.

The EDS elemental analyses are shown in Figure 25, and the weight percentage of the elements are presented in Table 5. The scale is mainly composed of magnesium (53.2 wt%), iodine (15 wt%), and oxygen with minor amounts of aluminum (6.1 wt%). The pocket material is mainly composed of aluminum (63 wt%), magnesium (17 wt%), and oxygen (13.9 wt%) with minor amounts of iodine (6.2 wt%). The elemental compositions of the bulk of the reference and exposed samples are the same within the experimental uncertainties.

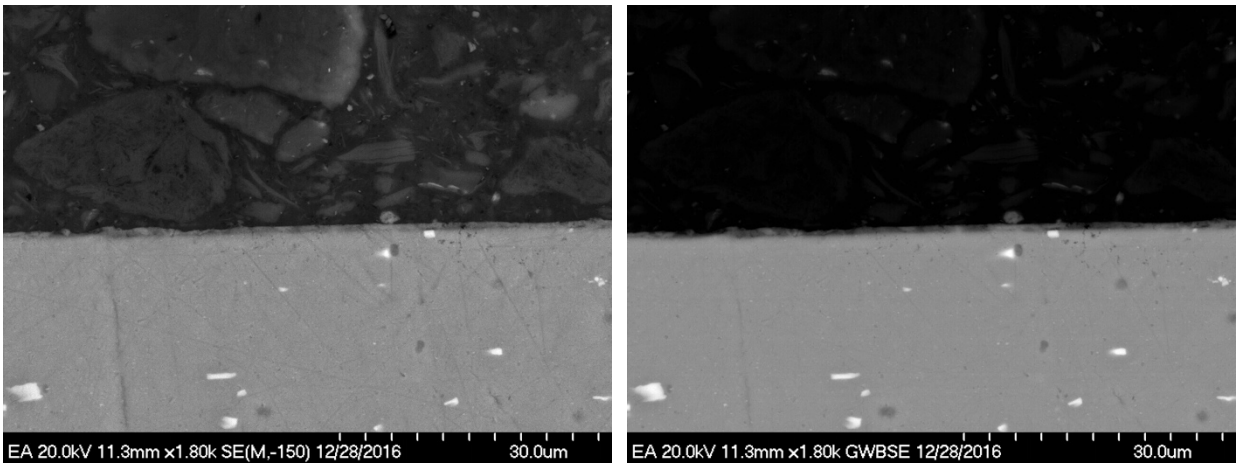

(a) (b)

Figure 23.—Cross-sectional reference 6061 aluminum alloy coupon sample. (a) SEM. (b) BSE.

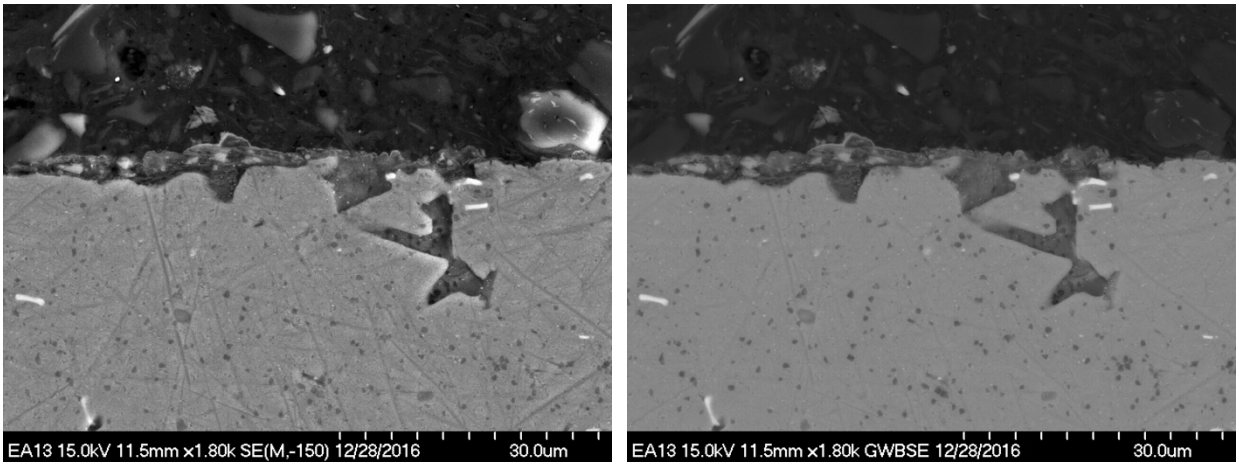

(a) (b)

Figure 24.—Cross-sectional 6061 aluminum alloy coupon sample exposed to iodine laminar vapor flow for 30 days. (a) SEM. (b) BSE.

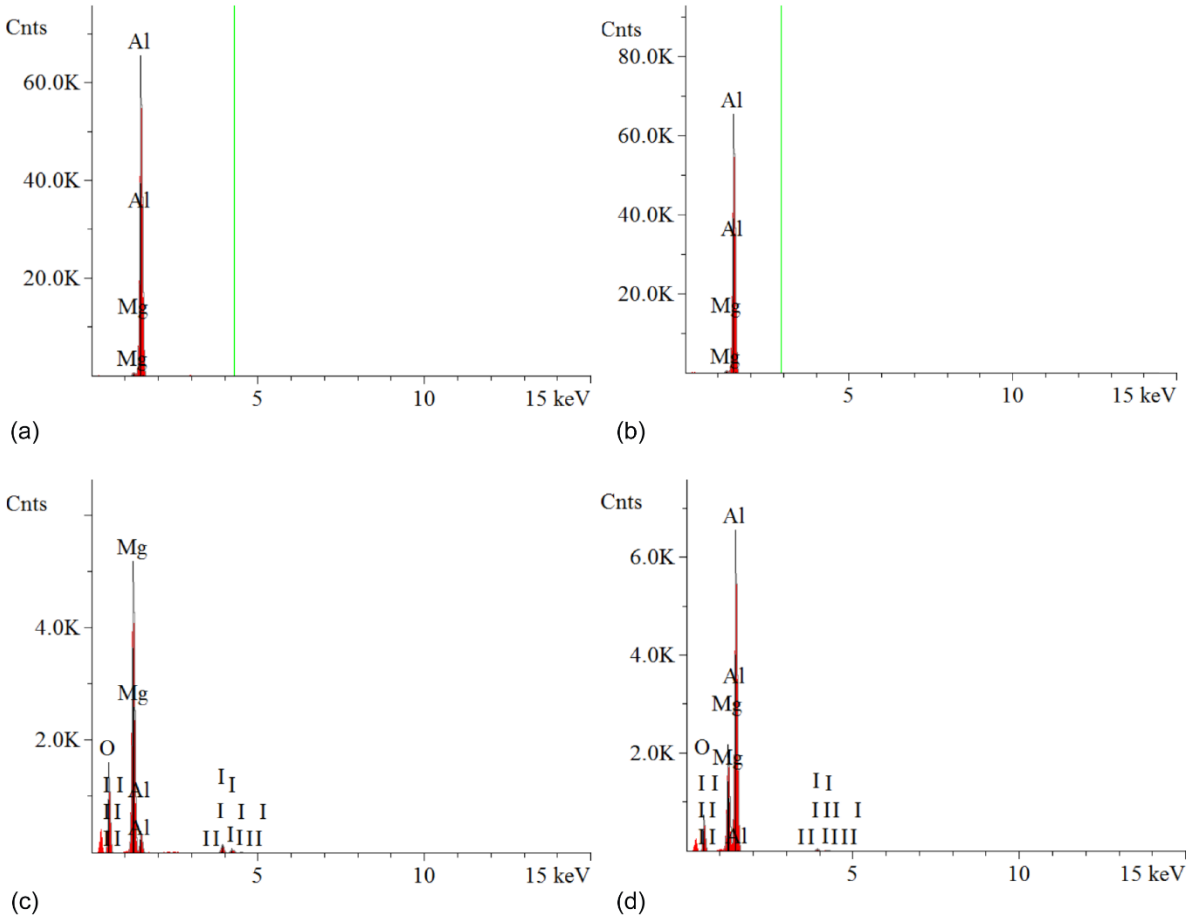

Figure 25.—EDS analysis of 6061 aluminum alloy samples. (a) Bulk of reference (Figure 23). (b) Bulk of exposed sample for 30 days (Figure 24). (c) Scale. (d) Pocket in bulk of sample.

TABLE 5.—CHEMICAL COMPOSITION OBTAINED FROM EDS ANALYSIS OF BULK OF REFERENCE AL-6061 SAMPLE AND BULK, SCALE, AND POCKET OF AL-6061 SAMPLE EXPOSED TO IODINE LAMINAR VAPOR FLOW FOR 30 DAYS

Element	Weight (%)			
	Reference	Exposed		
	Bulk	Bulk	Scale	Pocket
Al	98.8(3)	98.8(3)	6.1(3)	63.0(5)
Mg	1.22(3)	1.15(3)	53.2(5)	17.0(2)
I	---------	---------	15(1)	6.2(8)
O	---------	---------	25.3(5)	13.9(4)

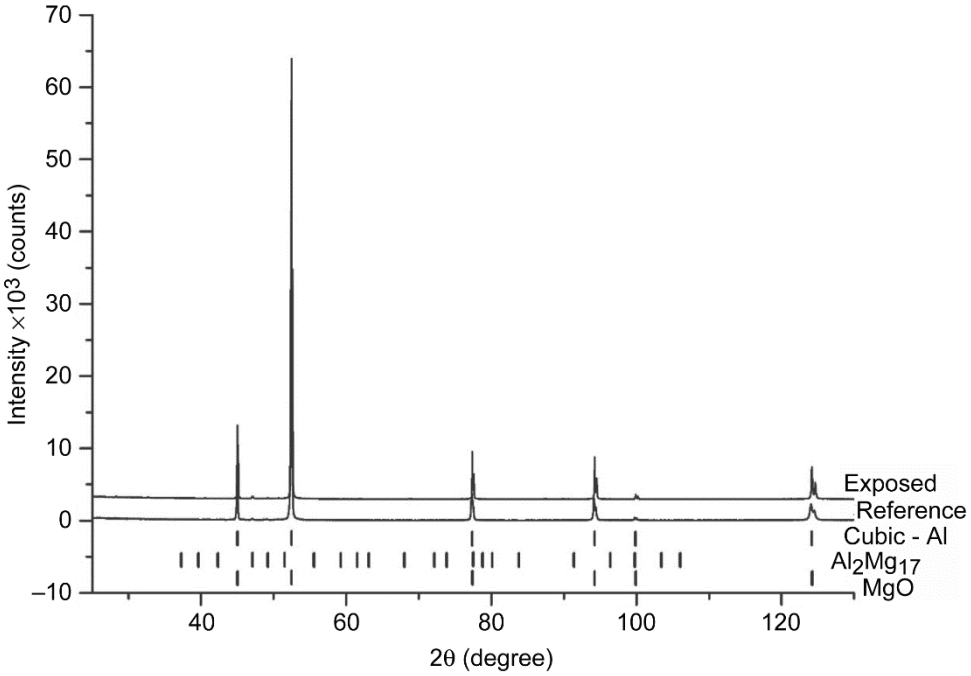

Figure 26.—X-ray diffraction patterns of 6061 aluminum alloy samples unexposed and exposed to iodine vapor laminar flow for 30 days.

The XRD patterns of the TiAl alloy samples both unexposed and exposed to iodine vapor for 30 days are presented in Figure 26. XRD analysis detected the aluminum (PDF card # 03-065-2869) and aluminum-magnesium ($Al_{12}Mg_{17}$, PDF card # 00-001-1128) phases in the as-received sample. Since the diffraction peaks of periclase (MgO, PDF # 98-000-5711) and aluminum phases overlap, we assume that the periclase phase is present in the scale of the sample based on the detection of magnesium and oxygen by EDS analysis.

Coatings on Alloys

The cross-sectional FIB images of the stainless steels 304 and 316 and the 6Al-4V titanium-aluminum coupon samples coated with Silcolloy® before and after exposure to the iodine vapor laminar flow at 300 °C for 30 days are shown in Figure 27, Figure 28, and Figure 29. The cross-sectional SEM and BSE images of the stainless steel 304 coated with Dursan® and carbon steel A36 coated with Silcolloy® coupon samples unexposed and exposed to iodine at the same conditions as described above are shown in Figure 30, Figure 31, Figure 32, and Figure 33. The thickness of the coatings are presented in Table 6. The thickness of the coatings remained approximately unaltered within the experimental uncertainties, except for the Sicolloy® coating on stainless steel 304 sample.

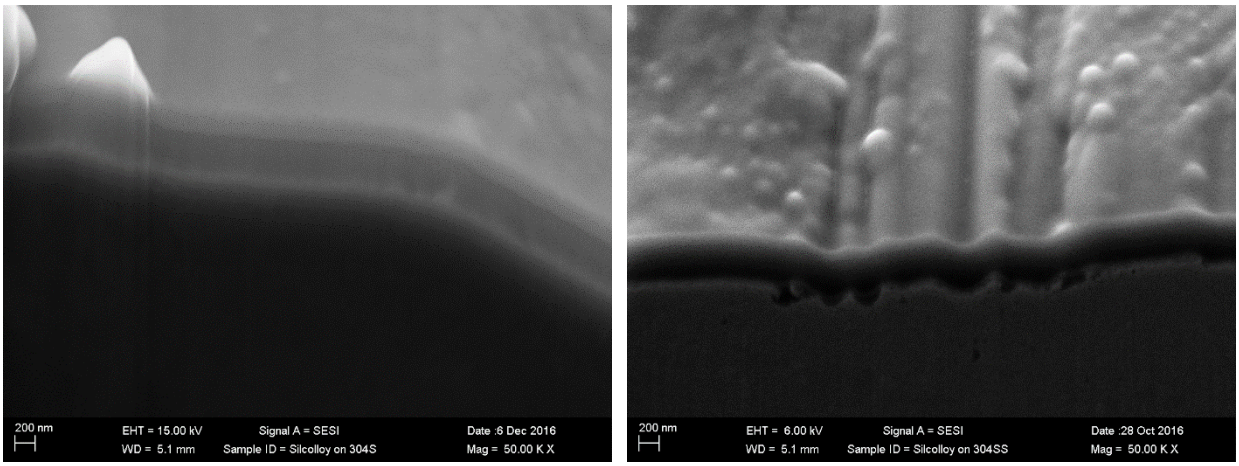

(a) (b)

Figure 27.—Cross-sectional FIB images of stainless steel 304 coupon sample coated with Silcolloy®. (a) Before exposure. (b) After iodine vapor laminar flow exposure for 30 days.

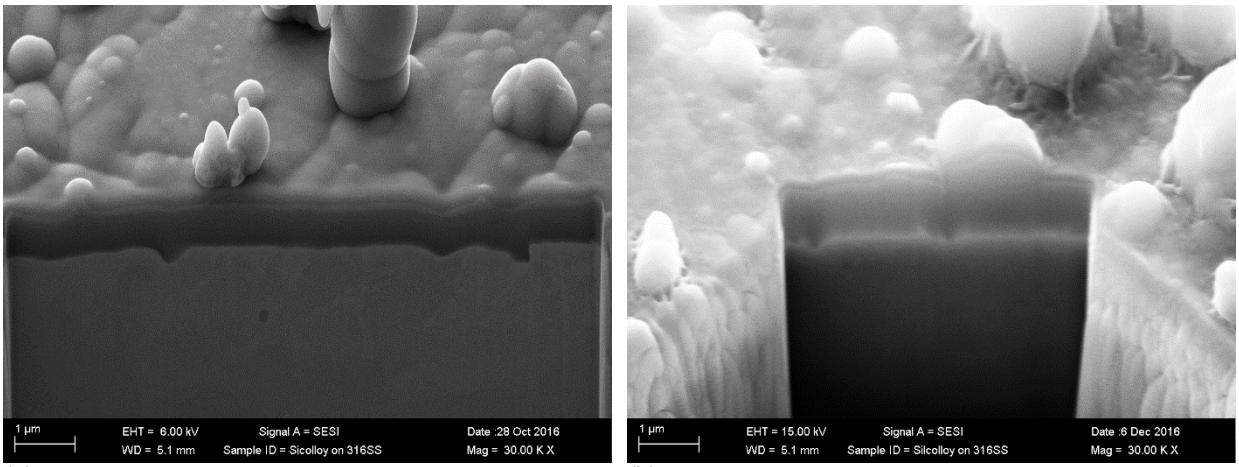

(a) (b)

Figure 28.—Cross-sectional FIB images of stainless steel 316 coupon sample coated with Silcolloy®. (a) Before exposure. (b) After iodine vapor laminar flow exposure for 30 days.

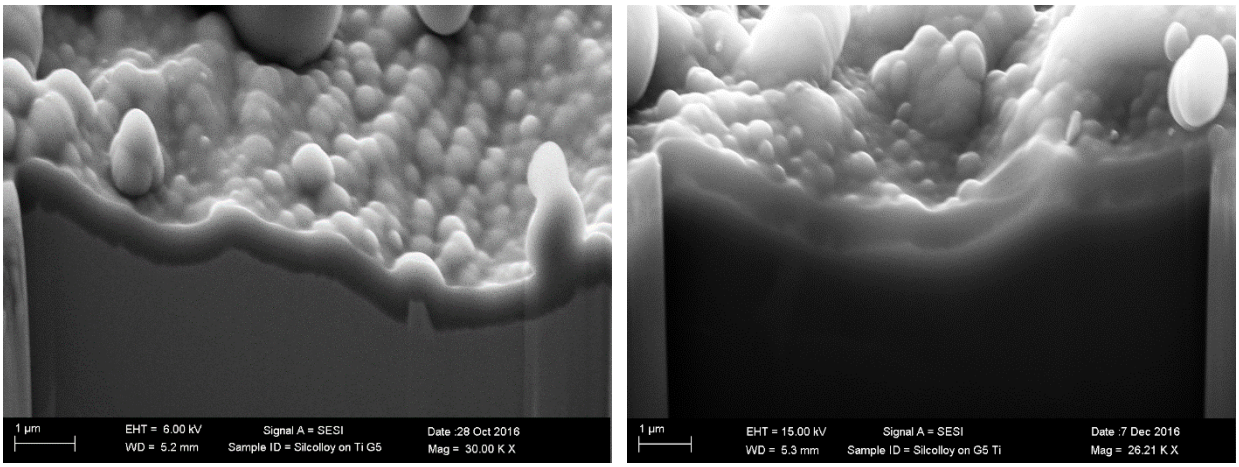

(a) (b)

Figure 29.—Cross-sectional FIB images of TiAl alloy coupon sample coated with Silcolloy®. (a) Before exposure. (b) After iodine vapor laminar flow exposure for 30 days.

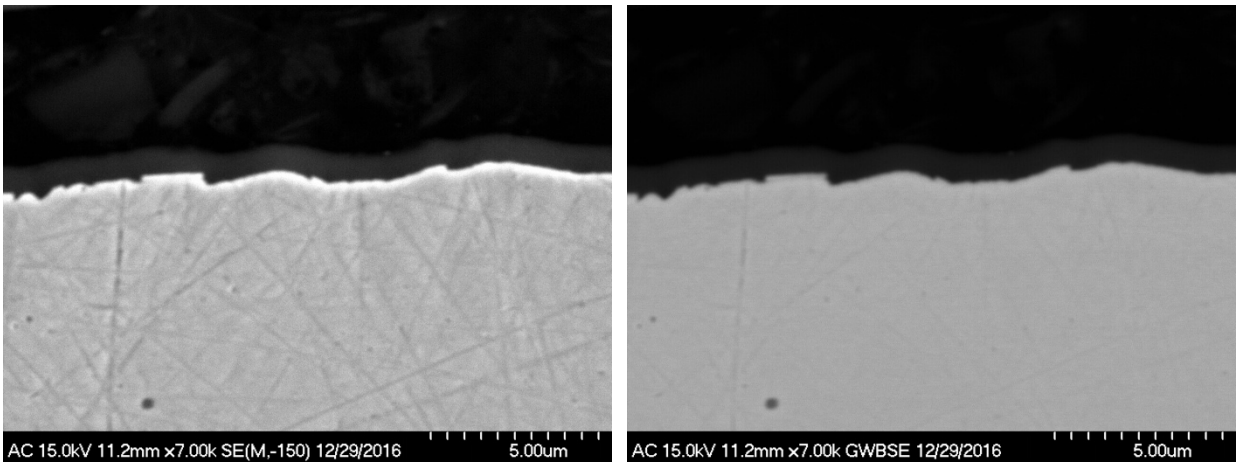

(a) (b)

Figure 30.—Cross-sectional Dursan® coating on stainless steel 304 sample. (a) SEM. (b) BSE.

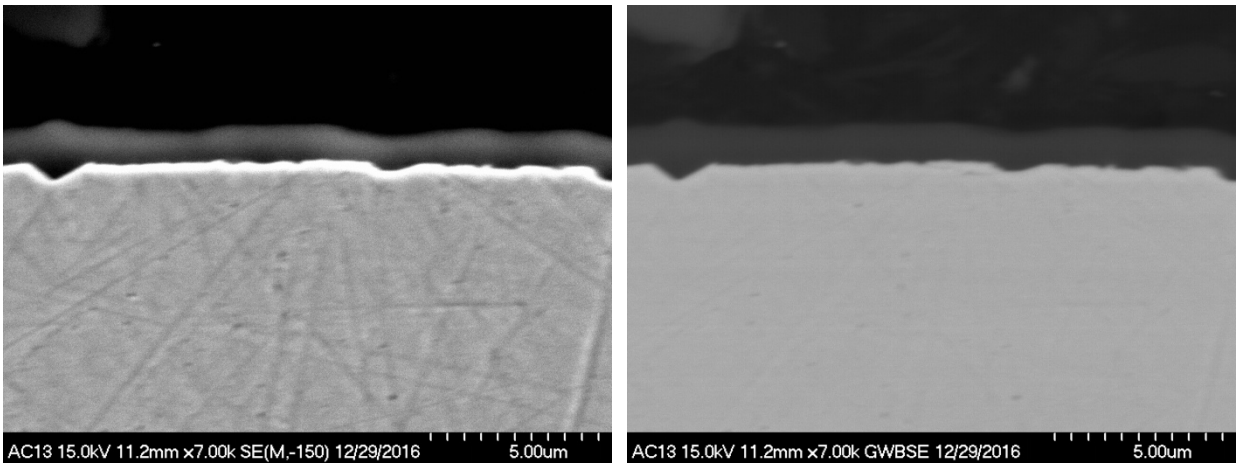

(a) (b)

Figure 31.—Cross-sectional Dursan® coating on stainless steel 304 sample exposed to iodine laminar vapor flow for 30 days. (a) SEM. (B) BSE.

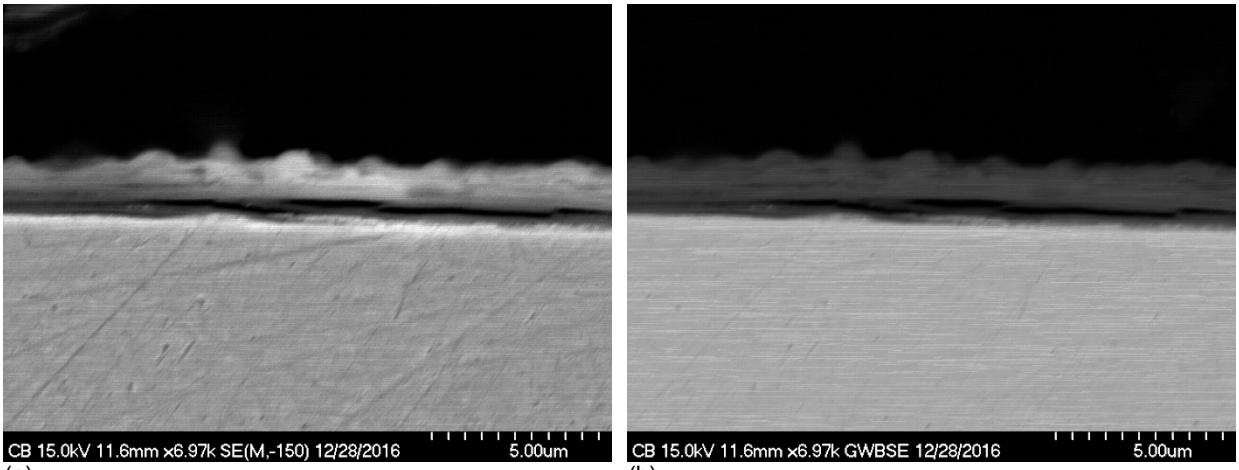

(a) (b)

Figure 32.—Cross-sectional Silcolloy® coating on A36 low carbon steel sample. (a) SEM. (b) BSE.

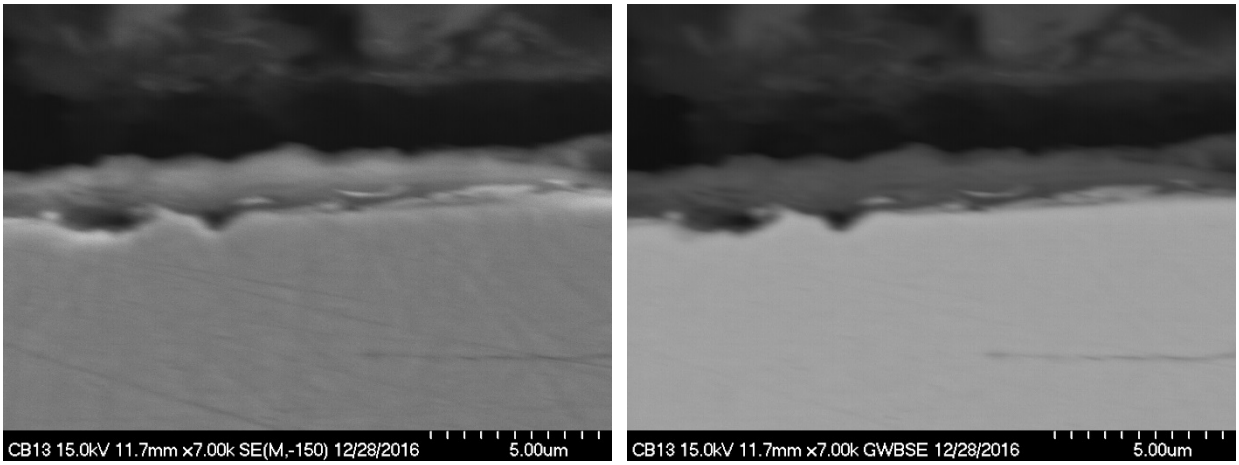

(a) (b)

Figure 33.—Cross-sectional Silcolloy® coating on A36 low carbon steel sample exposed to iodine laminar vapor flow for 30 days. (a) SEM. (b) BSE.

TABLE 6.—THICKNESS OF COMMERCIAL COATINGS SILCOLLOY® AND DURSAN® ON SS304 AND SS316, TiAl, AND AlMg BEFORE AND AFTER EXPOSED IN IODINE VAPOR LAMINAR FLOW AT 300 °C

Alloy	Coating	Thickness (nm)			
		Reference	±	30 days exposure	±
304	Silcolloy®	487	24	629	22
304	Dursan®	958	68	1000	50
316	Silcolloy®	1020	47	1094	36
A36	Silcolloy®	1509	88	1535	119
6Al-4V	Silcolloy®	711	15	939	51

The EDS elemental analyses of the stainless steels 304 and 316, A36 low carbon steel, and 6Al-4V titanium-aluminum alloy coupon samples coated with Silcolloy® and Dursan® exposed in iodine vapor laminar flow at 300 °C are shown in Figure 34, Figure 35, Figure 36, Figure 37, Figure 38, Figure 39, Figure 40, and Figure 41 and the weight percentage of the elements are presented in Table 7, Table 8, Table 9, Table 10, and Table 11. EDS elemental analysis of the coatings detected mainly silicon and oxygen in the Dursan® coating and mainly silicon in the Silcolloy® coating. The oxygen detected in the Dursan® coating is related to the oxygen present in the carboxysilane groups. Other elements (Fe, Cr, Ni, and Ti) detected in the coatings are originated from their diffusion from the substrate to the coating material during the deposition process or the exposure experiment. It is also possible that these elements detected in the coating are partially from the substrate since the beam size (0.5 to 1 μm diameter) and its excitation volume are larger than the thickness of the coatings. The content of iron in the Silcolloy® coating on stainless steels 304 and 316 samples after exposure increased 10 wt% and 14.1 wt%, respectively. The content of oxygen in this coating on stainless steels 304 and 316 and on A36 carbon steel samples after exposure also increased 18.8 wt%, 2.3 wt%, and 4.1 wt%, respectively. For the Silcolloy® coating on TiAl alloy after exposure, the content of titanium, aluminum, and oxygen in the coating increased 45.0 wt%, 2.5 wt%, and 0.8 wt%, respectively. Aluminum detected in Silcolloy® coating on stainless steel 304 may be due to the vapor deposition of formed aluminum iodide. Gallium detected by EDS in the samples analyzed by FIB microscopy are from the gallium ion milling used to obtain the cross-sectional features in the samples.

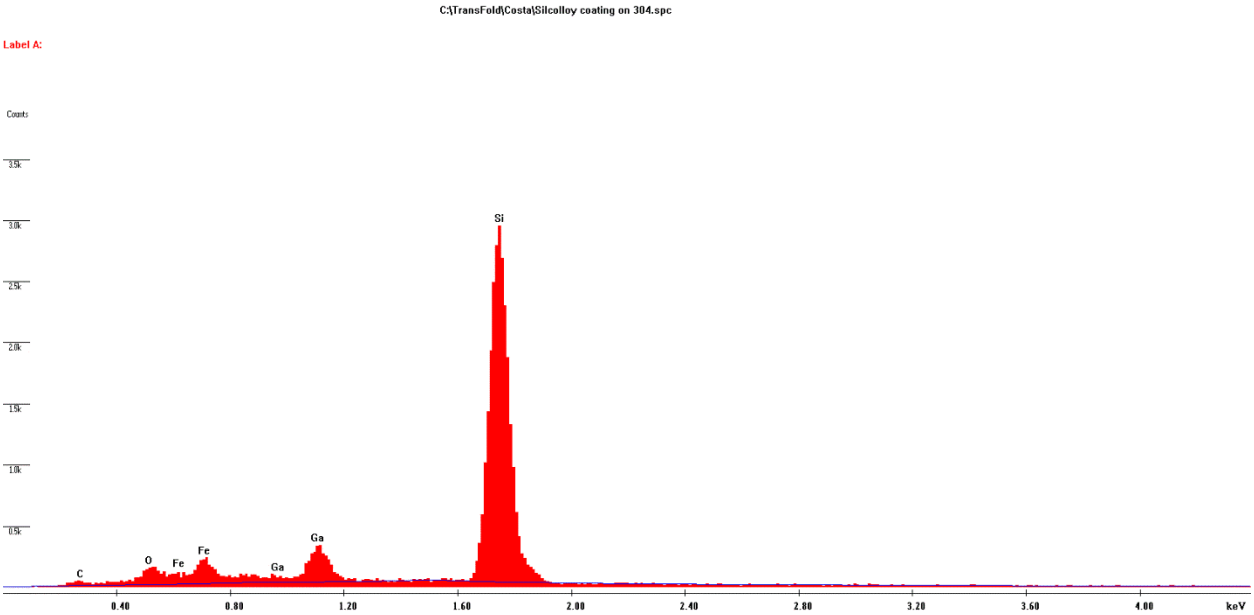

Figure 34.—EDS analysis of Silcolloy® coating on stainless steel 304 before exposure to iodine vapor laminar flow.

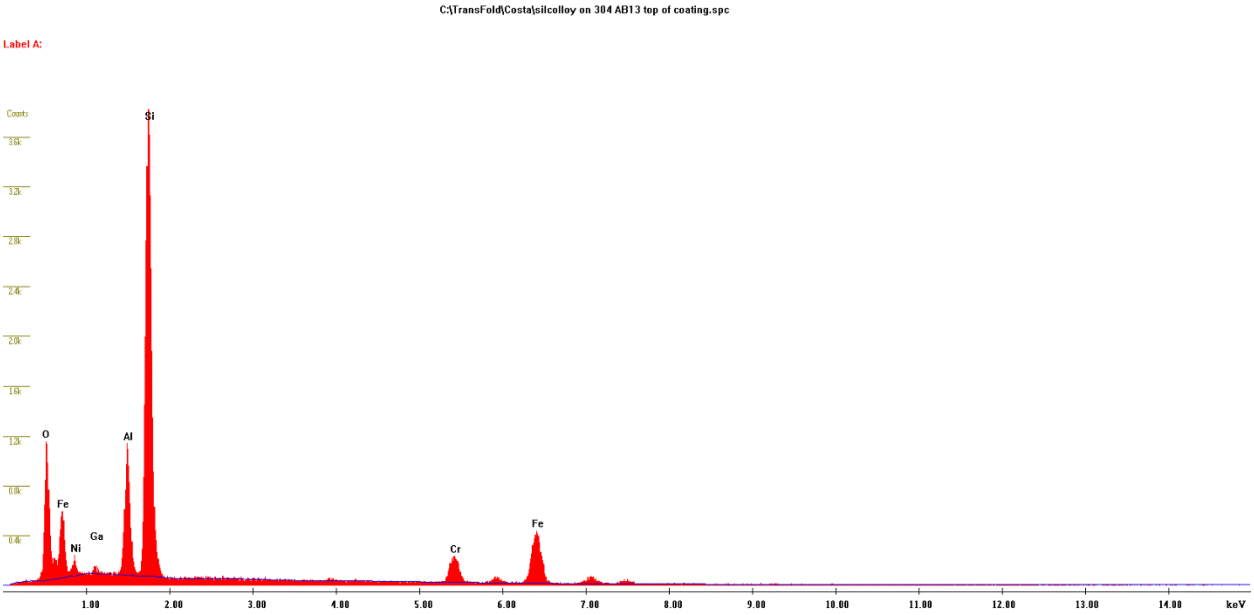

Figure 35.—EDS analysis of Silcolloy® coating on stainless steel 304 after exposure to iodine vapor laminar flow for 30 days.

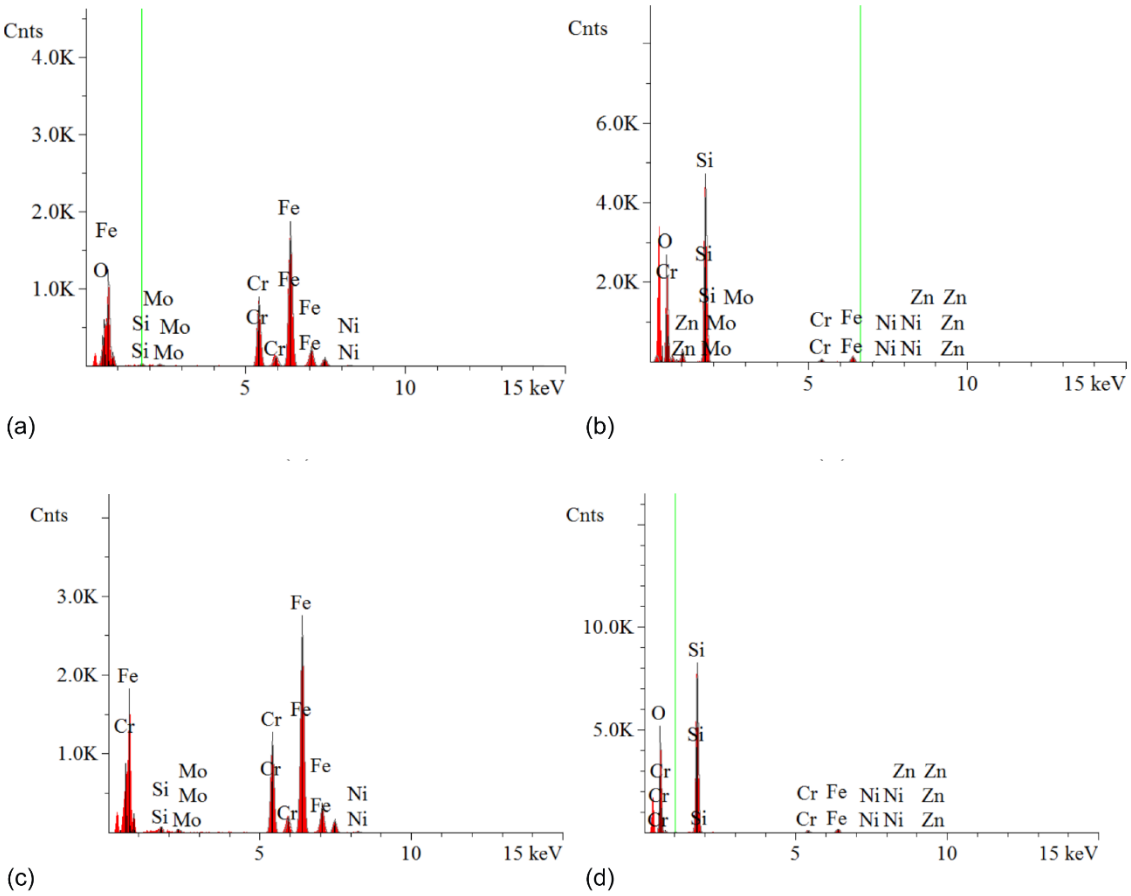

Figure 36.—EDS analysis of Dursan® coating on stainless steel 304 samples. (a) Bulk. (b) Coating of reference sample. (c) Bulk. (d) Coating of exposed sample for 30 days.

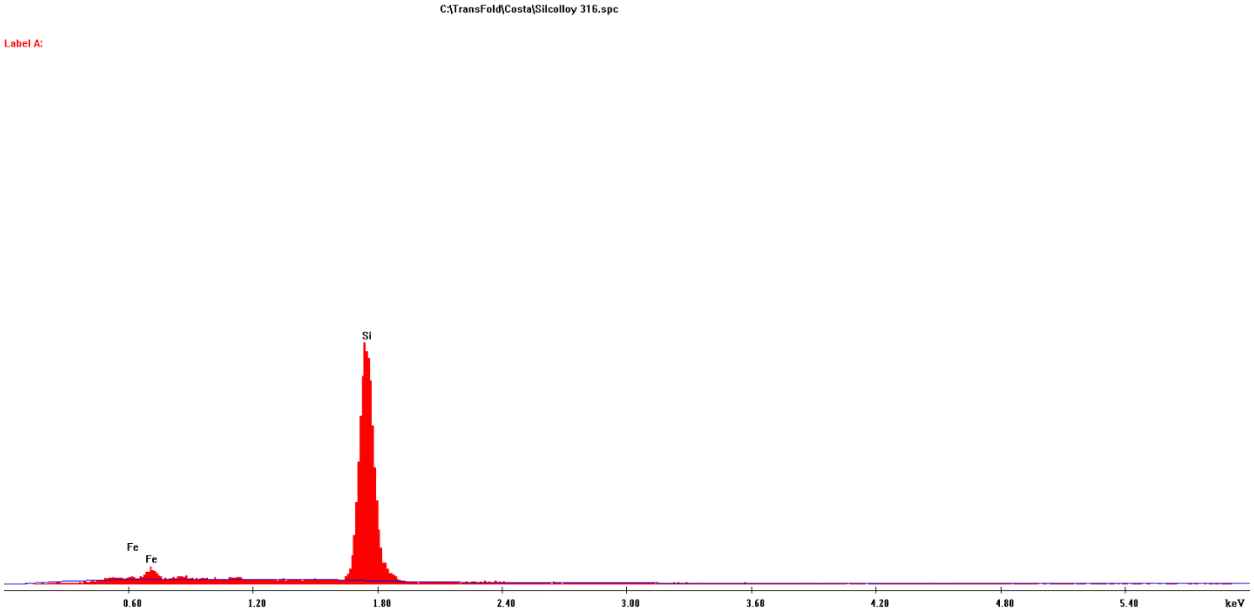

Figure 37.—EDS analysis of Silcolloy® coating on stainless steel 316 before exposure to iodine vapor laminar flow.

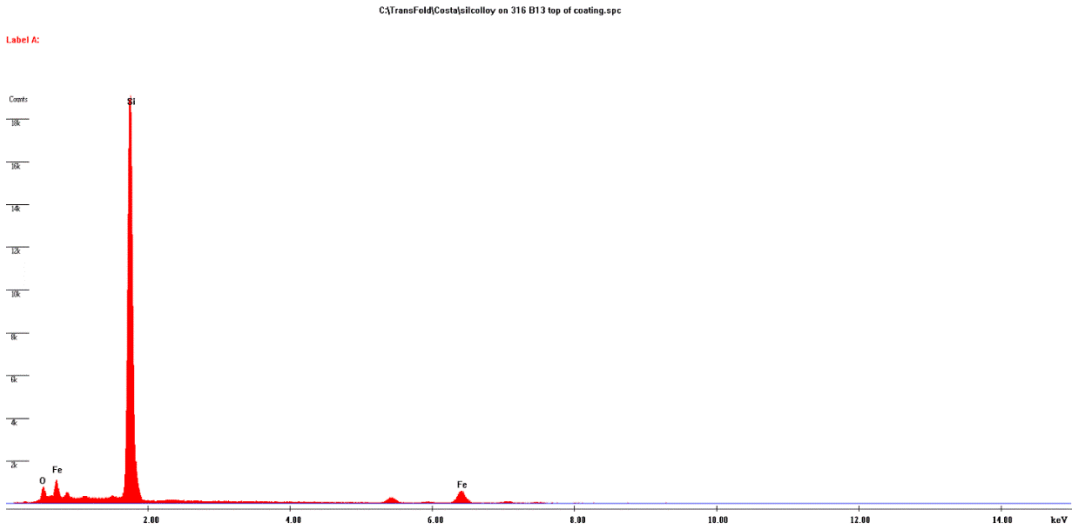

Figure 38.—EDS analysis of Silcolloy® coating on stainless steel 316 after exposure to iodine vapor laminar flow for 30 days.

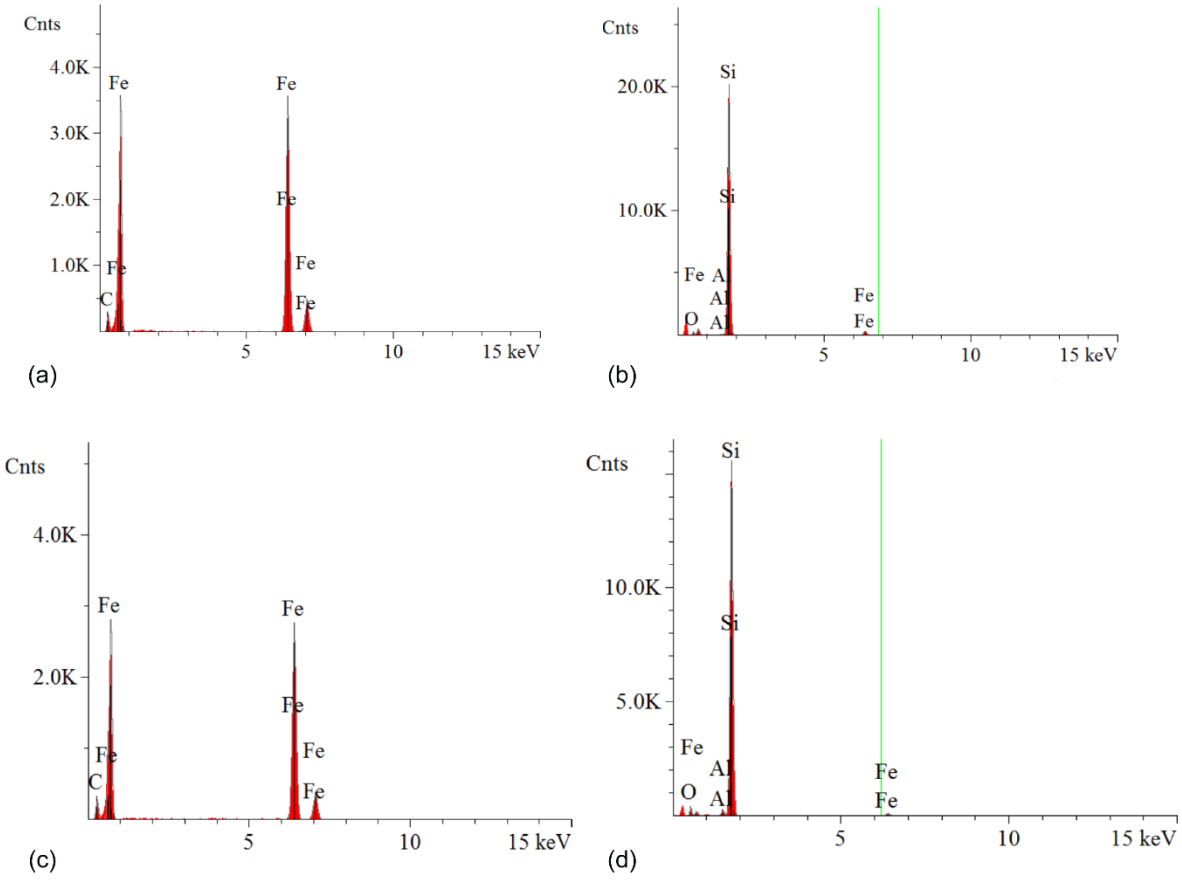

Figure 39.—EDS analysis of Silcolloy® coating on A36 low carbon steel samples. (a) Bulk. (b) Coating of reference sample. (c) Bulk. (d) Coating of exposed sample for 30 days.

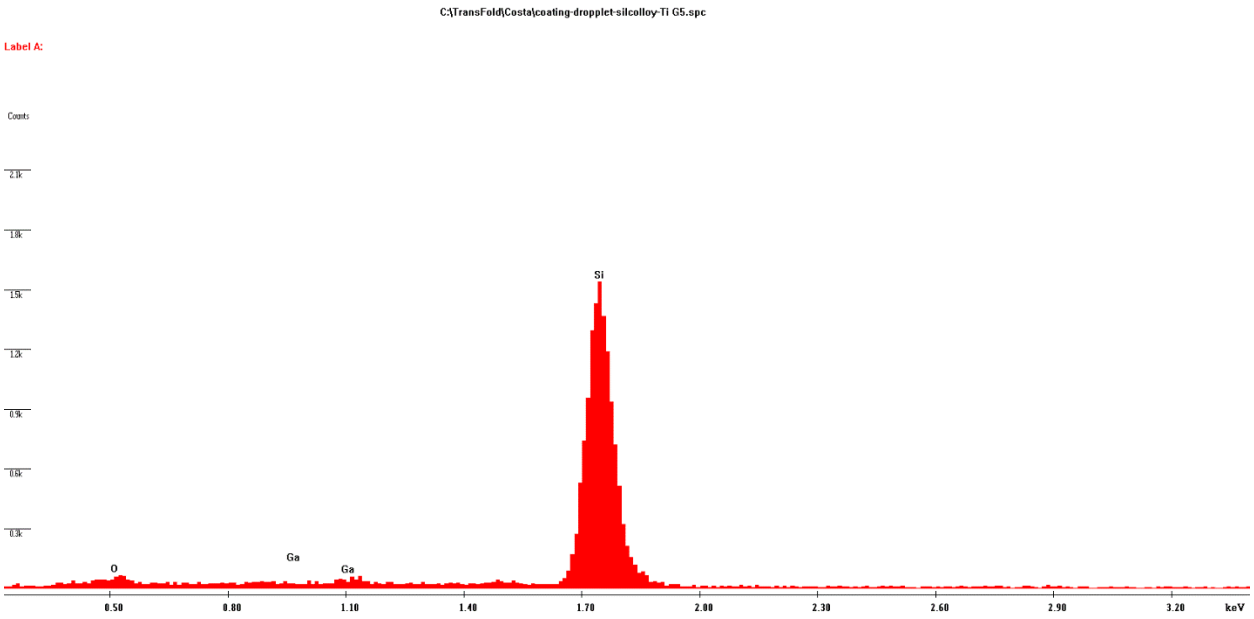

Figure 40.—EDS analysis of Silcolloy® coating on TiAl alloy sample before exposure to iodine vapor laminar flow.

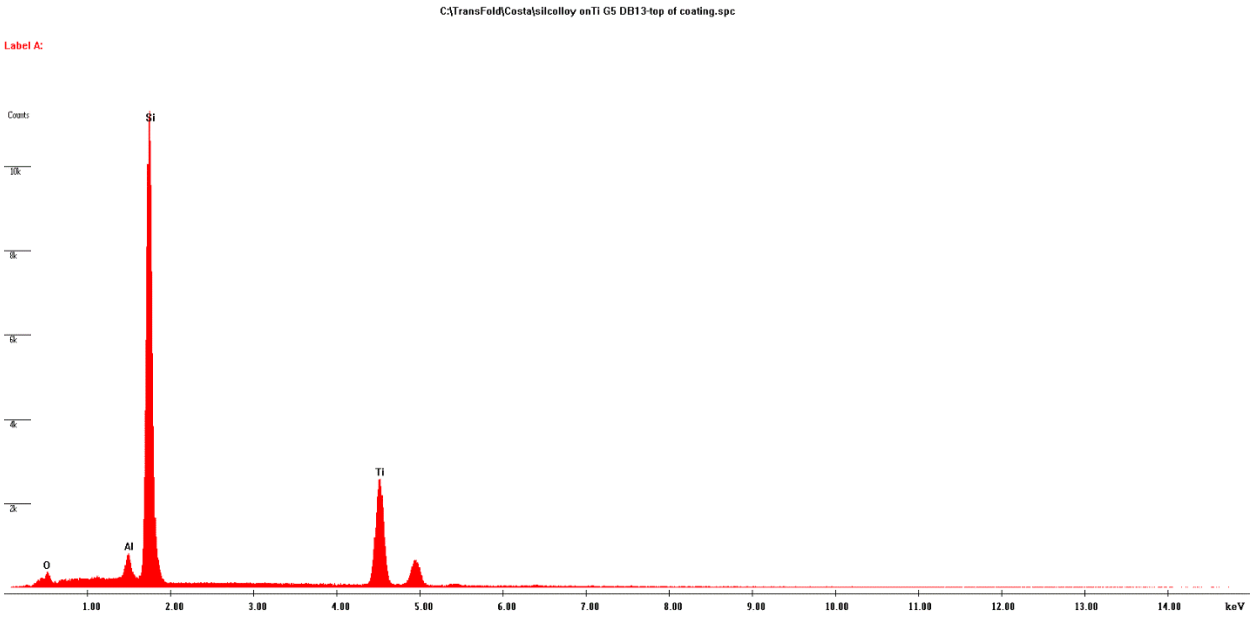

Figure 41.—EDS analysis of Silcolloy® coating on TiAl alloy sample after exposure to iodine vapor laminar flow for 30 days.

TABLE 7.—CHEMICAL COMPOSITION
OBTAINED FROM EDS ANALYSIS
OF SILCOLLOY® COATING
ON SS304 BEFORE AND AFTER
EXPOSURE TO IODINE VAPOR
LAMINAR FLOW FOR 30 DAYS

Element	Weight (%)	
	Before	After
Si	79.8	34.1
Fe	10.1	21.1
Al	-----	15.2
Cr	-----	6.5
Ni	-----	2.7
Ga	7.9	-----
O	1.6	20.4
C	0.6	-----

TABLE 8.—CHEMICAL COMPOSITION OBTAINED
FROM EDS ANALYSIS OF REFERENCE AND
EXPOSED SS304 SAMPLES
COATED WITH DURSAN®

Element	Weight (%)			
	Reference		Exposed	
	Bulk	Coating	Bulk	Coating
Fe	70.3(9)	5.2(2)	71.4(7)	4.3(2)
Cr	19.3(4)	2.2(1)	18.8(3)	1.9(1)
Ni	7.1(4)	0.5(1)	7.1(4)	0.4(1)
Zn	-------	0.9(2)	-------	-------
Mo	1.3(4)	-------	1.6(3)	-------
Si	0.8(2)	39.0(4)	1.1(1)	38.3(3)
O	1.1(2)	51.8(8)	-------	55.1(6)

TABLE 9.—CHEMICAL COMPOSITION OBTAINED
FROM EDS ANALYSIS OF SILCOLLOY® COATING
ON SS316 EXPOSURE TO IODINE VAPOR
LAMINAR FLOW FOR 30 DAYS

Element	Weight (%)	
	Before exposure	After exposure
Si	92.7	76.3
Fe	7.3	21.4
O	------	2.3

TABLE 10.—CHEMICAL COMPOSITION OBTAINED FROM EDS ANALYSIS OF REFERENCE AND EXPOSED A36 LOW CARBON STEEL SAMPLES COATED WITH SILCOLLOY®

Element	Weight (%)			
	Reference		Exposed	
	Bulk	Coating	Bulk	Coating
Fe	88.4(8)	6.6(2)	85.6(9)	3.1(2)
Si	----------	87.0(4)	----------	85.5(4)
Al	----------	0.45(6)	----------	1.34(8)
C	11.6(6)	----------	14.4(7)	----------
O	----------	5.9(4)	----------	10.0(5)

TABLE 11.—CHEMICAL COMPOSITION OBTAINED FROM EDS ANALYSIS OF SILCOLLOY® COATING ON TiAl ALLOY SAMPLES BEFORE AND AFTER EXPOSURE TO IODINE VAPOR LAMINAR FLOW FOR 30 DAYS

Element	Weight (%)	
	Before	After
Si	97.1	50.7
Ti	-----	45.0
Al	-----	2.5
Ga	1.8	-----
O	1.1	1.9

The XRD patterns of the stainless steel 304 samples coated with Silcolloy® that were unexposed and exposed to iodine for 30 days are presented in Figure 42. Only γ austenite (PDF card # 98-000-0258) and iron silicide (Fe0.95Si0.05, PDF # 04-003-7066) phases were detected by XRD analysis in the reference and exposed samples.

The XRD patterns of the stainless steel 304 samples coated with Dursan® that were unexposed and exposed to iodine for 30 days are presented in Figure 43. Only γ austenite (PDF card # 98-000-0258) and iron silicide ($Fe_{0.95}Si_{0.05}$, PDF # 04-003-7066) phases were detected by XRD analysis in the reference and exposed samples.

The XRD patterns of the stainless steel 316 samples coated with Silcolloy® unexposed and exposed to iodine for 30 days are presented in Figure 44. Only γ austenite (PDF card # 98-000-0258) and amorphous (amorphous hump around 32°) phases were detected by XRD analysis in the reference and exposed samples.

The XRD patterns of the A36 low carbon steel samples coated with Silcolloy® unexposed and exposed to iodine for 30 days are presented in Figure 45. Only α ferrite (PDF card # 98-000-1720) was detected by XRD analysis in the reference and exposed samples.

The XRD patterns of the TiAl alloy samples coated with Silcolloy® unexposed and exposed to iodine for 30 days are presented in Figure 46. XRD analysis detected the α phase (PDF card # 04-004-9156) and titanium suboxide phase ($TiO_{0.45}$, PDF card # 01-089-3074) in the as-received sample. Anatase (TiO_2, PDF card # 98-000-0081) phases were detected by XRD on the sample exposed in iodine vapor beyond the α and suboxide phases.

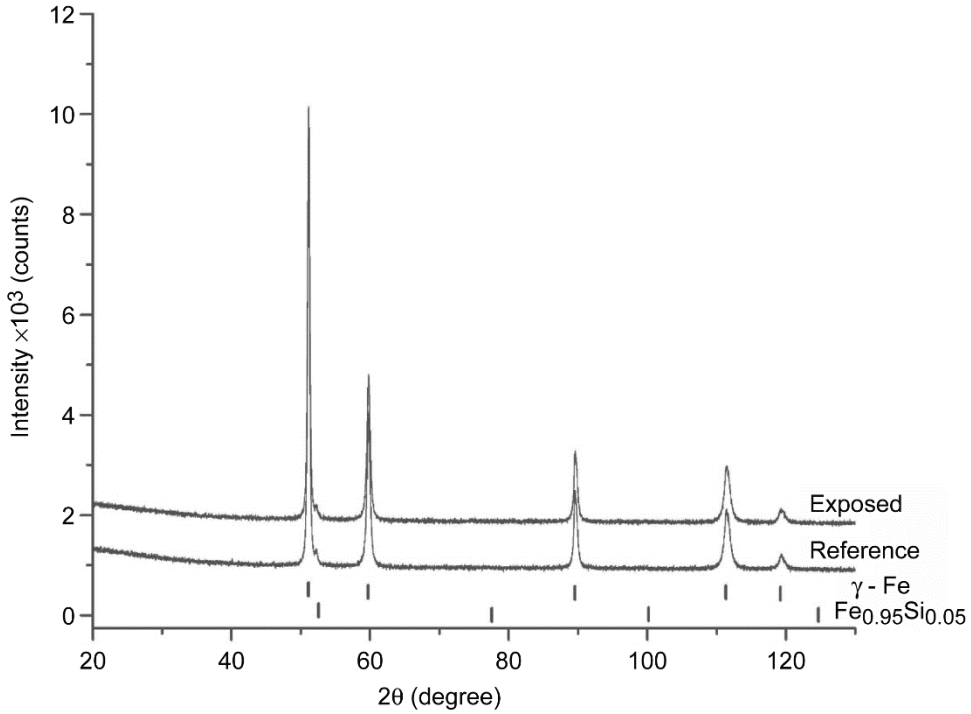

Figure 42.—X-ray diffraction patterns of stainless steel 304 samples coated with Silcolloy® unexposed and exposed to iodine vapor laminar flow for 30 days.

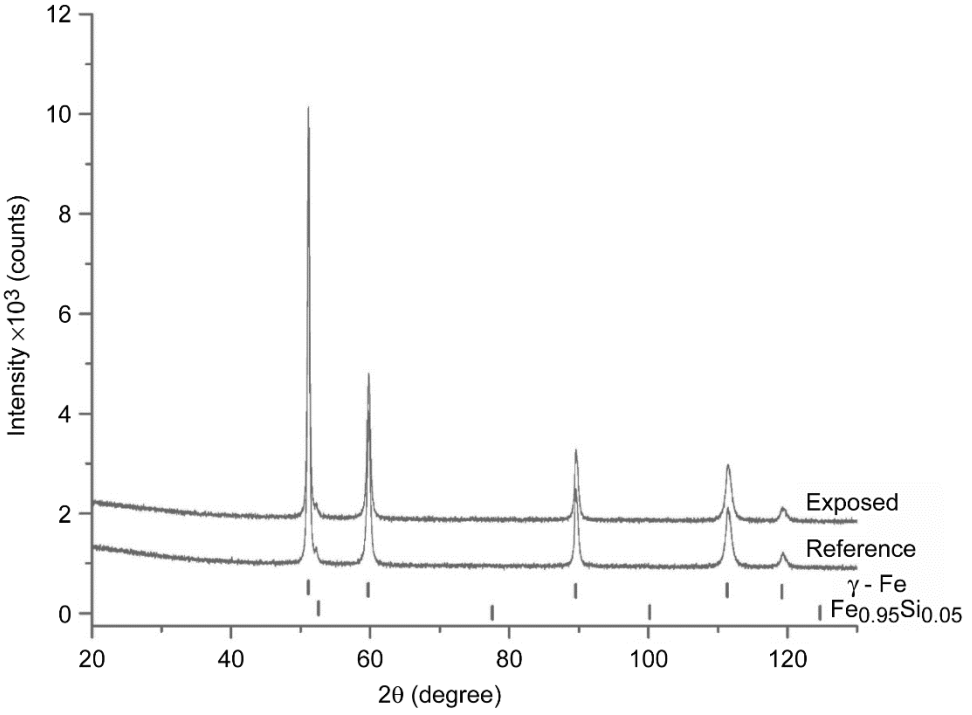

Figure 43.—X-ray diffraction patterns of stainless steel 304 samples coated with Dursan® unexposed and exposed to iodine vapor laminar flow for 30 days.

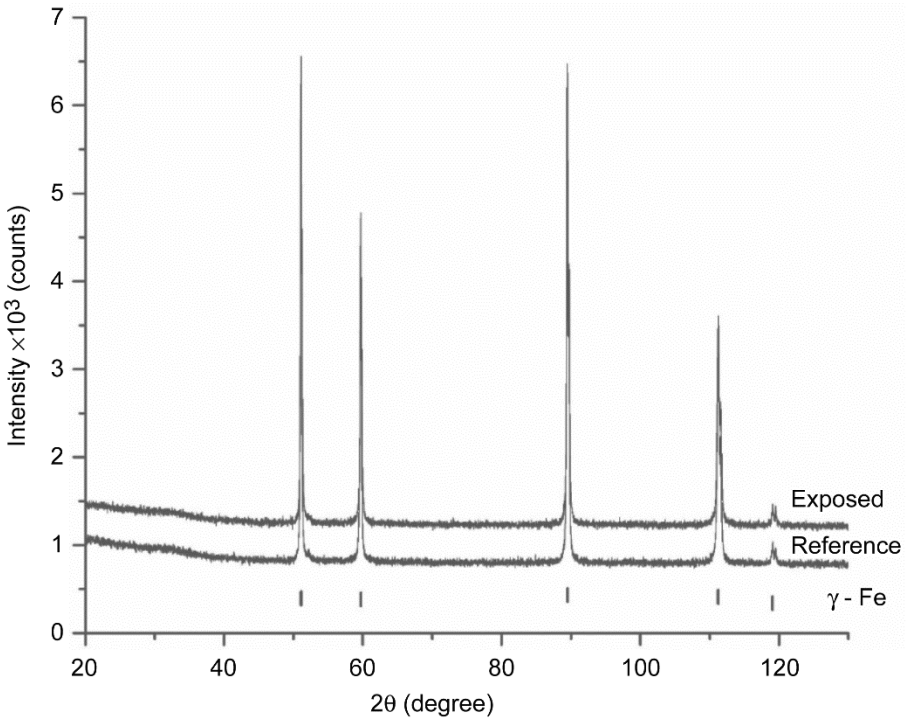

Figure 44.—X-ray diffraction patterns of stainless steel 316 samples coated with Silcolloy® unexposed and exposed to iodine vapor laminar flow for 30 days.

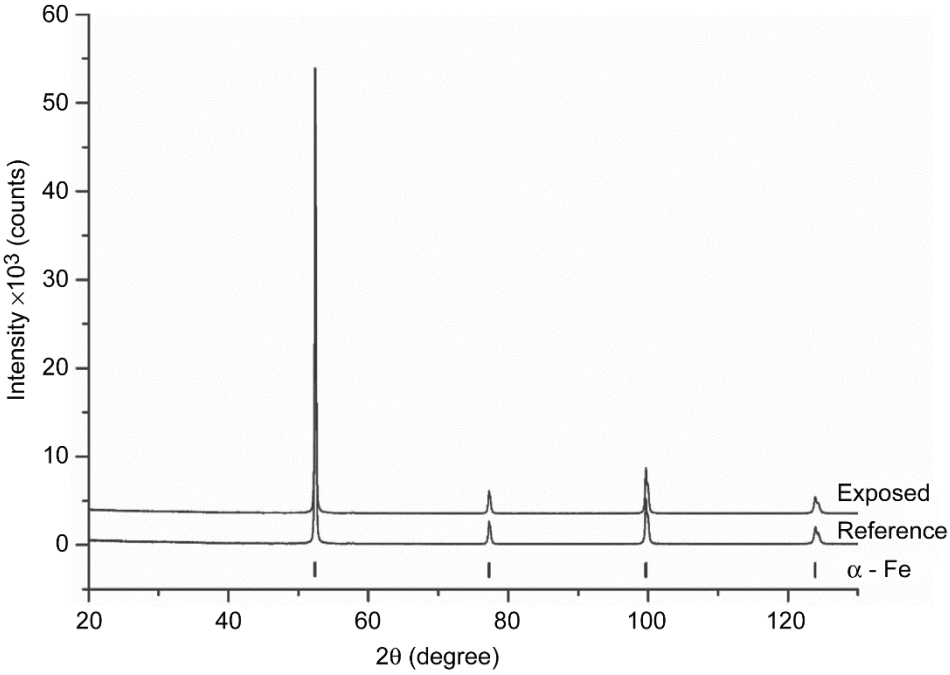

Figure 45.—X-ray diffraction patterns of A36 low carbon steel samples coated with Silcolloy® unexposed and exposed to iodine vapor laminar flow for 30 days.

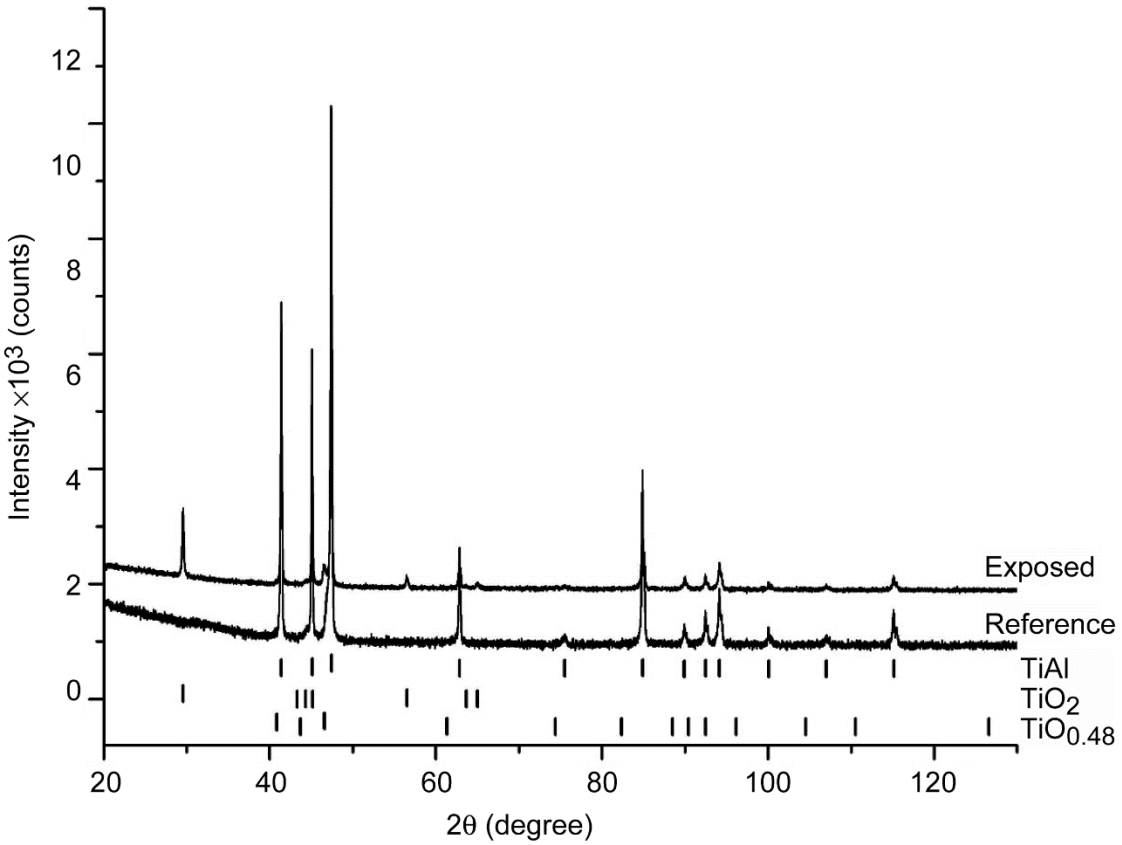

Figure 46.—X-ray diffraction patterns of TiAl alloy samples coated with Silcolloy® unexposed and exposed to iodine vapor laminar flow for 30 days.

Discussion

The thermodynamic stability of some preferential compounds formed, assuming that the contribution of the kinetics effects are negligible here, can be calculated by computational thermochemistry tools. We use the FactSage free energy minimization program and associated databases (Refs. 4 and 5) as a thermochemistry computational tool to calculate the main compounds formed at their thermodynamic equilibrium when the alloy samples are exposed to iodine vapor containing or not containing oxygen. We used the infinite amounts of the iodine (10^5 g) with and without oxygen (10^3 g), and the initial amounts and the thermodynamic activities of iron, chromium, nickel, titanium, aluminum, and magnesium in the alloys at 300 °C (573 K) and 1 atm as input parameters into the free energy minimizer program (Table 12). The thermodynamic activities of the alloy components listed in Table 13 were calculated using Thermo-Calc and its SGTE Solutions Database (SSOL6). The results of the FactSage calculations are shown in Table 14. For simplicity of the results, only the predicted thermodynamically stable compounds having activities equal 1 are listed in Table 14 and their calculated amounts (g) are omitted here.

TABLE 12.—AMOUNT OF CHEMICAL SPECIES USED AS INPUT PARAMETERS IN THERMODYNAMIC CALCULATIONS OF COMPOUNDS FORMED ON SAMPLES EXPOSED TO IODINE OR IODINE PLUS OXYGEN

Sample	Amount 10^2(g)[a]						
	Fe	Cr	Ni	C	Ti	Al	Mg
304	74	17.9	8.3	-	-----	-----	-----
316	70	16.3	10.5	-	-----	-----	-----
A36	97	-----	-----	3	-----	-----	-----
TiAl	-----	-----	-----	-	92.4	7.2	-----
AlMg	-----	-----	-----	-	-----	98.8	1.22

[a]Measured by EDS analysis (wt%).

TABLE 13.—THERMODYNAMIC ACTIVITIES USED AS INPUT PARAMETERS IN FACTSAGE

Sample	Thermodynamic Activities						
	Fe	Cr	Ni	C	Ti	Al	Mg
304	0.932	0.980	0.119	--------	--------	--------	--------
316	0.932	0.980	0.119	--------	--------	--------	--------
A36	1.000	--------	--------	1.000	--------	--------	--------
TiAl	--------	--------	--------	--------	0.842	$2.53 \cdot 10^{-9}$	--------
AlMg	--------	--------	--------	--------	--------	0.980	0.0549

TABLE 14.—COMPARISON OF PREDICTED THERMODYNAMICALLY STABLE COMPOUNDS TO THOSE COMPOUNDS, PHASES, AND ELEMENTS DETECTED BY EDS ANALYSIS AND XRD DIFFRACTION

Alloy	Phases detected by XRD	Elements detected by EDS[b]	Predicted thermodynamically stable compounds	
			Pure iodine	100 I_2:1O_2 mass ratio
SS304	$FeNiCrO_4$, Fe_2O_3	Bright area – Fe and O Dark area – Fe, Cr, Ni and O	CrI_2(s)	Cr_2O_3(s), CrI_2(s)
SS316	$FeNiCrO_4$, Fe_2O_3	Fe, Cr, Ni and O	CrI_2(s)	Cr_2O_3(s), CrI_2(s)
A36	Fe_3O_4 and $Fe_{2.66}O_4$	Outer layer – Fe and O Middle layer – Fe, C and O Inner layer – Fe, and O	FeI_2(s) and C(graphite)	FeI_2(s,g), Fe_2O_3(s) and C(graphite), CO_2(g), CO(g), I(g), I_2(g), $(FeI_2)_2$(g)
TiAl	$TiO_{0.48}$ and TiO_2	Ti, Al, I and O[a]	TiI_2(s)	TiI_2(s) and α-TiO(s)
AlMg	MgO	Mg, Al, I and O	MgI_2(s)	MgI_2(s) and periclase MgO(s)

[a]EDS analysis of yellowish material deposited on inner walls at end of quartz tubular furnace.
[b]Elements with weight percent less than 4 percent are omitted here.

Austenitic and Carbon Steel

The products formed on the steel coupon samples exposed to iodine vapor laminar flow are mainly oxides ($FeNiCrO_4$ and Fe_2O_3 from stainless steels 304 and 316 and Fe_3O_4 from carbon steel A36). The predicted thermodynamically stable compounds derived from FactSage are in good agreement with phases and elements detected by EDS and XRD diffraction techniques except for stainless steels 304 and 316. This discrepancy between the predicted and detected phases/compounds may be indication that the reactions between the elements of the alloy and the gaseous phase is more kinetically governed. Only small amounts of iodine were detected by EDS at the interface between the oxides and the base of the stainless steels 304 and 316. The formation of oxides on the base of the alloys clearly indicates that oxygen was present in the iodine vapor flow in the RIG system. Oxygen might have been introduced to the system during the beginning of the experiment when an empty Erlenmeyer flask was replaced by the one containing solid iodine. It is also possible that oxygen came from the high purity argon cylinder. It is well known that even high purity argon contains oxygen at ppm level, which would be enough to cause oxidation at the extension observed in our studies. Considering oxygen was present in our system, our experimental findings are in good agreement to those reported by Wren et al. (Ref. 6) who proposed that corrosion of stainless steel exposed to iodine and air at room temperature is catalyzed by iodine. In their study, gaseous iodine was adsorbed and desorbed on stainless steel at room temperature and the surface of the samples were analyzed by EDS and by X-ray photoelectron spectroscopy. They found a preferential diffusion of iron and the formation of Fe-I-O and proposed the following reactions between stainless steel, air, and iodine.

$$Fe_{FeCrNi} + I_2(g) = FeI_2(s) \tag{1}$$

$$FeI_2(s) + \frac{y}{2}O_2(g) = FeI_xO_y(s) + \left(1 - \frac{x}{2}\right)I_2(g) \tag{2}$$

in which FeI_xO_y is composed of iron iodides and iron oxides. They also stated that the FeI_xO_y phase mixture could react with more oxygen to release iodine. Their findings corroborate well with our results obtained by XRD and EDS analysis although our samples were exposed to a higher temperature (300 °C) and in a much lower oxygen partial pressure. The fact that XRD analysis detected only $FeNiCrO_4$ and Fe_2O_3 phases in the stainless steel samples may be related to the detection limit of this technique (~1 wt%) considering that small amounts (2 to 4 wt%) of elemental iodine were detected by EDS in the scale of the stainless steel samples. It is also possible that iodine is adsorbed on the oxides of the scale. The formation of $FeNiCrO_4$ indicates that iron, nickel, and chromium initially reacts with iodine and are further oxidized to $FeNiCrO_4$ and Fe_2O_3. Any iodide or iodate compounds formed would be carried by the iodine-argon flowing gases since these compounds in solid or liquid phases are volatile and also may have low decomposition temperatures (e.g., $Fe(IO_3)_3$ decomposes at 130 °C) (Refs. 3 and 7). This reaction releases more iodine according to the reaction in Equation (2) as it was proposed previously by Wren et al. (Ref. 6) resulting in oxides with very low contents of iodine. For carbon steel A36, the main product of the reaction Fe_3O_4 and the absence of iodine indicates that FeI_2 was completely converted to the oxide phase.

Although additional data points, especially at short exposition times, would be required to calculate the oxidation kinetics of the steel samples, it is possible to postulate that the last three data points of the weight gain per area in Figure 4 related to the oxidation of the steel samples that would fit into a parabolic rate equation. The parabolic rate law describes a mass increase of a sample, which is the case for oxidation of steels in this study. In this case, the rate of this reaction is mainly dominated by Equation (2). From Figure 4, we conclude that the resistance of the steels to iodine and oxygen corrosion increases in the order carbon steel A36 > stainless steel 304 > stainless steel 316. The highest corrosion resistance of stainless steel 316 is related to its highest nickel content. Since iron preferentially diffuses to the surface for reaction, any effect leading to a decrease in the iron activity would increase the corrosion resistance of

the alloy. As it is well known, the activity of iron diminishes as the nickel content in an alloy increases. Here, the stainless steel 316 has the highest content of nickel (stainless steel 316, 11 wt%; stainless steel 304, 8 wt%; and carbon steel A36, 0 wt%) and thus it would exhibit the lowest iron activity and higher corrosion resistance to iodine and oxygen atmosphere.

Aluminum- and Titanium-Based Alloys

The absence of scale on the TiAl alloy sample exposed to iodine for 30 days indicates that metallic iodide (M_xI_y, M = Al^{3+}, and Ti^{4+}) compounds are the main products of the reaction between TiAl alloy sample and iodine vapor. Although these iodide compounds are solid phases, they exhibit elevated vapor pressures and might be carried by the laminar iodine flow. Note that the relative small peak intensities of the secondary TiO_2 phases in the XRD diffractograms indicates small amounts of TiO_2 formed on the surface of the TiAl alloy. This indicates that oxygen partial pressure of oxygen in the rig system was not high enough to completely oxidize the Ti and $TiO_{0.48}$ to TiO_2 to form protective scales. Furthermore, a yellowish deposit found to be formed on the inner walls of the quartz furnace is another strong indication of the formation of volatile iodide compounds. EDS analysis confirmed that this deposit is mainly composed of titanium, aluminum, iodine, and oxygen. In very low oxygen partial pressures, which is the case of this study, iodine vapor reacts with TiAl according to the reactions (Ref. 8).

$$\mathrm{Ti_{TiAl} + I_2(g) = TiI_2(s)} \tag{3}$$

$$\mathrm{TiI_2(s) + O_2 = TiO_2(s) + I_2(g)} \tag{4}$$

The weight loss per area of the TiAl would be governed by Equation (3) and the best equation describing the net weight loss per area of the sample (Figure 5) would be a paralinear rate equation originally derived by Tedmon (Ref. 9) and also used by Maloney and McNallan (Ref. 10) to describe two simultaneous reactions between chlorine, oxygen, and cobalt at 927 °C (1200 K) leading to increase (oxide scale growth and parabolic) and decrease (oxide consumption and linear) of sample mass. The differential equation describing this rate of change is

$$\frac{dx}{dt} = \frac{K_d}{x} - K_s \tag{5}$$

where x is the thickness of the scale, K_d is the parabolic rate constant of the scale growth (cm^2/s), and K_s is the linear rate constant of the scale thickness decrease (cm/s).

The higher content of magnesium compared to the lower content of aluminum in the scale of the AlMg alloy sample indicates that magnesium is preferentially reacting with iodine and then is converted to oxide. It is also possible that aluminum is reacting to iodine to form aluminum iodine and then is further oxidized to oxide. From XRD diffraction, it was not possible to confirm if the scale formed was composed of magnesium oxide since its diffraction peaks overlap with the diffraction peaks of aluminum. Alumina was also not detected by XRD, which might be related to lower detection limit of the diffractometer and the small amounts of the scale formed. Based on the experimental findings of this study and on the thermodynamic calculations reported by Donchev et al. (Ref. 8) the following reactions can be assumed for the reaction between the AlMg alloy sample, iodine, and oxygen.

$$\mathrm{Mg_{AlMg} + I_2(g) = MgI_2(s)} \tag{6}$$

$$\mathrm{MgI_2(s) + 1/2O_2 = MgO(s) + I_2(g)} \tag{7}$$

$$Al_{AlMg} + 3/2I_2(g) = AlI_3(l) \quad (8)$$

$$AlI_3(l) + 3/2O_2 = Al_2O_3(s) + I_2(g) \quad (9)$$

The weight loss per area of the AlMg alloy sample (Figure 5) suggests that the reaction is mostly governed by Equations (6) and (8) followed by volatilization of their products MgI_2 and AlI_3. The paralinear law also would be the most adequate equation to fit the data points of Figure 5.

Silcolloy® and Dursan® Coatings

Silcolloy® deposited on stainless steel 316, carbon steel A36, and 6Al-4V TiAl alloy, and Dursan® applied on stainless steel 304, were effective in protecting the surface of the alloys against iodine-catalyzed oxygen corrosion. Stainless steel 304 coated with Silcolloy® was the only exception of protecting the base of alloy against corrosion by iodine. This conclusion is based on the sample exposed to iodine vapor for 30 days, which exhibited a small increase (1.02 ± 0.07 mg cm^{-2}) in the mass of the sample and in the thickness (142 ± 33 nm) of the Silcolloy® coating. We suspect that the coating failure to protect the base of the alloy may be related to surface preparation before coating deposition and coating deposition process since this coating worked well in protecting the base of the other alloys. Further studies addressing surface preparation and the coating deposition process are needed to address this issue.

The iron silicide crystalline phases detected by XRD analysis on the stainless steel 304 samples coated with Dursan® and Silcolloy® are originated from the reaction of silicon from the coating with iron from the base of the alloy during the deposition process. The results obtained by XRD analysis corroborate well with those obtained by EDS analysis. From EDS analysis, we also conclude that the constituent's elements of alloys diffuse to the coating although not changing its corrosion protective characteristics.

Conclusions

Weight Gain Per Area

The weight gain per area performance of the materials exposed in iodine laminar flow with oxygen at impurity levels are from the lowest to the highest weight gain per area as follows:

(1) No weight change was observed for stainless steel 316, low carbon steel A36, and Ti-Al alloy coated with Silcolloy® (SilkoTek Corporation) and stainless steel 304 coated with Dursan® (SilkoTek Corporation)
(2) Steels: < 316 < 304 < A36
(3) Ti-Al-Mg-based alloys: Al-Mg < Ti-Al

Stainless Steels 304 and 316

From XRD and EDS analysis, it was found that scales formed on the stainless steels 304 and 316 consist of hematite (Fe_2O_3) and spinel ($FeNiCrO_4$) crystalline phases. The corrosion process, which is catalyzed by iodine, is governed by the reaction between iron iodide and oxygen forming iron, chromium, and nickel oxides.

Low Carbon Steel A36

The main crystalline phases formed on the base of the low carbon steel are magnetite and carbon graphite. The corrosion of this sample is also similar to those observed for stainless steels 304 and 316 in which iron first reacts with iodine (catalyzed) followed by oxidation to magnetite (Fe_3O_4) and release of iodine.

Ti-Al-Mg Alloys

Only a very thin film of anatase TiO_2 was formed on Ti-Al alloy. The corrosion reactions on TiAl are mostly governed by the reaction between titanium and aluminum in the alloy, and iodide to give titanium and aluminum iodide volatile compounds, which are carried by the laminar flow of iodine and argon at 300 °C.

A scale consisting mainly of aluminum, iodine, and oxygen formed on the Al-Mg sample exposed to 30 days. Some pockets rich in magnesium, iodine, and oxygen also formed in this Al-Mg alloy. Magnesium preferentially reacts with iodine to form magnesium iodide, which is oxidized by oxygen to magnesium oxide. Aluminum follows the same reaction mechanisms. Both aluminum and magnesium reactions are governed by their conversion to iodide compounds, which are carried by the laminar flow of iodine and argon at 300 °C.

Silcolloy® and Dursan®

Silcolloy® was effective in protecting the stainless steel 316, low carbon steel A36, and Ti-Al alloy against corrosion of the iodine containing oxygen atmosphere at 300 °C. Stainless steel 304 coated with Silcolloy® exposed for 30 days did not exhibit corrosion although the sample gained weight and the coating exhibited expansion. Further research work on surface preparation and finishing is needed to address this anomaly.

Dursan® was effective in protecting the stainless steel 304 against corrosion of the iodine containing oxygen atmosphere at 300 °C.

References

1. Smith, Timothy D., et al.: Overview of NASA Iodine Hall Thruster Propulsion System Development. NASA TN30748, 2016.
2. Hillier, Adam C.: Revolutionizing Space Propulsion Through the Characterization of Iodine as Fuel for Hall-Effect Thrusters. Thesis, Air Force Institute of Technology, AFIT/GA/ENY/11–M08, 2011.
3. Polzin, Kurt A., et al.: Propulsion System Development for the Iodine Satellite (iSAT) Demonstration Mission. Proceedings of the 30th ISTS and 34th IEPC, 2015.
4. Bale, C.W., et al.: FactSage Thermochemical Software and Databases, 2010–2016. CALPHAD: Computer Coupling of Phase Diagrams and Thermochemistry, vol. 54, 2016, pp. 35–53.
5. Bale, C.W., et al.: FactSage Thermochemical Software and Databases. Calphad, vol. 26, 2002, pp. 189–228.
6. Wren, J.C.; Glowa, G.A.; and Merritt, J.: Corrosion of Stainless Steel by Gaseous I2. J. Nucl. Mater., vol. 265, 1999, pp. 161–177.
7. Lide, D.R.: CRC Handbook of Chemistry and Physics. 71st ed., CRC Press, Boca Raton, FL, 1990.
8. Donchev, A.; Gleeson, B.; and Shütze, M.: Thermodynamic Considerations of the Beneficial Effect of Halogens on the Oxidation Resistance of TiAl-based Alloys. Intermetallics, vol. 11, 2003, pp. 387–398.
9. Tedmon, C.S.: The Effect of Oxide Volatilization on the Oxidation Kinetics of Cr and Fe-Cr Alloy. J. Electrochem. Soc., vol. 113, 1966, pp. 766–768.
10. Maloney, M.J.; and McNallan, M.J.: The Effect of Chlorine on the Kinetics of Oxidation of Colbalt in Environments Containing 0.5 Atmosphere of Oxygen between 900 K and 1200 K. Metall. Trans. B, vol. 16, 1985, pp. 751–761.